Journal of Sound and Vibration (2000) **237**(3), 483–511
doi:10.1006/jsvi.2000.3064, available online at http://www.idealibrary.com on IDEAL®

PASSIVE AND ACTIVE ISOLATION OF STRUCTURAL VIBRATION TRANSMISSION BETWEEN TWO PLATES CONNECTED BY A SET OF MOUNTS

P. GARDONIO† AND S. J. ELLIOTT

Institute of Sound and Vibration Research, University of Southampton, Southampton SO17 1BJ, England. E-mail: pg@isvr.soton.ac.uk

(*Received* 10 *November* 1999, *and in final form* 4 *May* 2000)

This paper introduces the theory of an impedance-mobility matrix model used to predict the structural vibration transmission between two plates, which are mechanically coupled via an active mounting system. With this model the active and passive isolation effectiveness of different types of mounting systems has been studied. In particular, the case of a three-mount isolator system with inertial or reactive actuators has been investigated in order to assess the influence of the mount stiffness and of the presence of rigid elements (block masses) at each end of the mounts. Three cost functions have been investigated: first, the minimization of the total structural power transmitted by the source to the receiver; second, the cancellation of out-of-plane input velocities to the receiver and third the cancellation of out-of-plane input forces to the receiver. The simulations carried out have shown that the best passive and active isolation are both achieved when soft mounts are used. The number of mounts and the presence of block masses at each end of the mounts significantly affect the passive isolation but have shown a smaller influence on the active isolation. The three control strategies studied have shown similar active control effectiveness in all cases examined and for both inertial or reactive control actuators. The validity of the model has also been assessed by comparing the predicted levels of vibration transmission with and without control with measured data taken from a laboratory experiment.

1. INTRODUCTION

The work summarized in this paper forms part of a collaborative research programme to investigate the structure- and air-borne sound transmission through the double-wall structure of aircraft or helicopters. The goal of this project is to develop modelling techniques to predict accurately the structure- and air-borne sound transmission through a general structure of this type. This paper deals specifically with the theoretical analysis of structural vibration transmission through an array of active mounts which are the only connection between two plates.

The problem of structure-borne noise transmission between flexible mechanical systems connected via a set of mounts cannot be studied using the standard mathematical models given in reference [1] which consider the mounting system as a single lumped spring in parallel with a damper. A more detailed model is needed which accounts for the effects of multiple mounts and for the effects of multiple-degrees-of-freedom (d.o.f.s) vibration transmission at the connecting points. Also, the distributed nature of the source and receiver structures and some isolator components has to be taken into account so that coupling

†Author to whom correspondence should be addressed.

0022-460X/00/430483 + 29 $35.00/0

effects between the vibration components related to different types of waves propagating in the elements of the three systems is accounted for.

The finite element method (FEM) [2], could be employed for this type of study but it generates large matrix models that require very long simulations for a relatively small frequency range of analysis, even when the latest personal computer or work stations are used. Two alternative approaches are more suitable for structure-borne noise transmission problems at audio frequencies. The first one is the statistical energy analysis (SEA) approach [3]. This approach is based on power transmission concepts using coupling factors between source and receiver structures assuming the two structures to be of either infinite or semi-infinite extent. This simplification allows the prediction of the vibration level of the source and receiver structures with a relatively simple matrix model that could be utilized up to high frequencies (several kHz) with relatively fast computer simulations. The simplification introduced by the SEA approach of neglecting the resonant effect of the source and receiver structures could lead to some problems in the so-called low–mid-frequency range below about 1 kHz, particularly if the effects of active control devices such as an active mounting system are under study. The second approach based on impedance and mobility matrices (IMM), has therefore been considered so that the resonant behaviour of the three elements and the multiple d.o.f.s vibration transmission at the junctions of each element can be accounted for in the calculations with a relatively simple matrix model.

The SEA [4] and IMM approaches have both been used in this project so that two tools were available for the understanding of the passive and active isolation effects produced by the mounting system studied and developed in the project. In this paper, the simulations carried out with a matrix model based on point and transfer mobilities or impedances is presented [5]. This model considers the system divided into three elements: the source, the mounting system and the receiver. These elements are assumed to be connected at a finite number of point junctions at which multi d.o.f.s vibration transmission occurs. The three elements are modelled as distributed one- or bi-dimensional systems in which structural waves can propagate. The mounts are modelled as passive rubber elements with either a reactive or an inertial control actuator which have been represented, respectively, by a pair of reactive forces applied at each end of the mounts or by a sky hook control force applied at one end of the mounts. The effects of some parts of the mounting systems or of the source and receiver systems can also be included in the model as lumped masses, springs and dampers.

The vibration of the source and receiver systems has been expressed in terms of kinetic energy. In particular, an estimate of the kinetic energy represented by the square values of the out-of-plane velocities at five points on the source and receiver plates has been calculated so that the estimate of kinetic energy derived from experimental measurements taken on those points can be compared with the results obtained with the simulations.

This mathematical model allows the study of different control strategies by considering the minimization of a quadratic cost function. In particular, the effect of cancelling either the axial velocity or axial force at the top of the mount has been compared with the optimal control approach of minimizing the total power transmitted from the source to the receiver.

The effect of the mounts stiffnesses and the effects of lumped masses attached at each end of the mounts has also been assessed. Finally, a comparison between the results obtained here with those from an experimental investigation are also presented.

2. MATRIX MODEL FOR AN ACTIVE ISOLATING SYSTEM

In references [6–19] different types of mathematical models are described for the study of isolator systems composed of a source of vibration, a transmitting system and a receiver

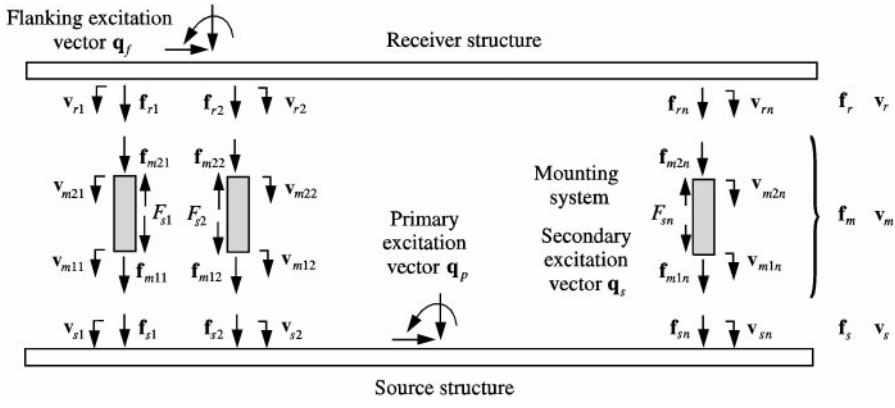

Figure 1. Scheme of a general complete isolating system.

structure. Each of these models considers in detail some aspects of the vibration transmission. This section describes the mobility-impedance matrix model used to derive the steady state response to harmonic excitation of the isolator system considered in this paper. With this model it is possible to consider the following features of an isolator system: first, the effects due to a flexible and distributed source as well, mounting and receiver structures; second, the effects generated by a multiple mounting isolator system and third, the multiple d.o.f.s vibration transmission at the junctions of each mount.

The complete isolating system is divided into three flexible parts as shown in Figure 1: the source, the mounting system, composed of n elements, and the receiver. These parts are connected at a finite number of junctions. At each junction, the motion and the forces transmitted are characterized by six complex parameters at a single frequency of excitation, which is characterized by a time dependence of the form $\exp(j\omega t)$. These velocity and force parameters are grouped in a velocity junction vector and a force junction vector which, for the jth junction can be written as

$$\mathbf{v}_j^{\mathrm{T}} \equiv \{\dot{u}_j \;\; \dot{v}_j \;\; \dot{w}_j \;\; \dot{\theta}_{xj} \;\; \dot{\theta}_{yj} \;\; \dot{\theta}_{zj}\}, \quad \mathbf{f}_j^{\mathrm{T}} \equiv \{N_{xj} \;\; N_{yj} \;\; N_{zj} \;\; M_{xj} \;\; M_{yj} \;\; M_{zj}\}, \tag{1,2}$$

where $\dot{u}_j$, $\dot{v}_j$, $\dot{w}_j$ are the complex linear velocities, respectively, along the x, y and z directions, $\dot{\theta}_{xj}$, $\dot{\theta}_{yj}$, $\dot{\theta}_{zj}$ are the complex angular velocities referred, respectively, to the x-, y- and z-axes, N_{xj}, N_{yj}, N_{zj} are the complex forces in the x, y and z directions and finally M_{xj}, M_{yj}, M_{zj} are the complex moments referred, respectively, to the x-, y- and z-axes.

With reference to the notation shown in Figure 1, combinations of these junction vectors are then grouped together to form three combined pairs of vectors: the *source velocity vector* ($\mathbf{v}_s$) and *force vector* ($\mathbf{f}_s$), the *receiver velocity vector* ($\mathbf{v}_r$) and *force vector* ($\mathbf{f}_r$) and the *mounting system velocity vector* ($\mathbf{v}_m$) and *force vector* ($\mathbf{f}_m$). The source and receiver velocity vector and force vector are given by

$$\mathbf{v}_s \equiv \begin{Bmatrix} \mathbf{v}_{s1} \\ \mathbf{v}_{s2} \\ \vdots \\ \mathbf{v}_{sn} \end{Bmatrix}, \qquad \mathbf{f}_s \equiv \begin{Bmatrix} \mathbf{f}_{s1} \\ \mathbf{f}_{s2} \\ \vdots \\ \mathbf{f}_{sn} \end{Bmatrix}, \qquad \mathbf{v}_r \equiv \begin{Bmatrix} \mathbf{v}_{r1} \\ \mathbf{v}_{r2} \\ \vdots \\ \mathbf{v}_{rn} \end{Bmatrix}, \qquad \mathbf{f}_r \equiv \begin{Bmatrix} \mathbf{f}_{r1} \\ \mathbf{f}_{r2} \\ \vdots \\ \mathbf{f}_{rn} \end{Bmatrix}, \tag{3–6}$$

where $\mathbf{v}_{sj}$, $\mathbf{f}_{sj}$ represent the velocity and the force junction vectors at the source junction for the jth mount, while $\mathbf{v}_{rj}$, $\mathbf{f}_{rj}$ represent the velocity junction vector and the force junction

vector at the receiver junction for the jth mount. The vectors of velocities and forces of the mounting system are given by

$$\mathbf{v}_m^{\mathrm{T}} \equiv \{\mathbf{v}_{m11}^{\mathrm{T}} \;\; \mathbf{v}_{m12}^{\mathrm{T}} \;\; \cdots \;\; \mathbf{v}_{m1n}^{\mathrm{T}} \;\; \mathbf{v}_{m21}^{\mathrm{T}} \;\; \mathbf{v}_{m22}^{\mathrm{T}} \;\; \cdots \;\; \mathbf{v}_{m2n}^{\mathrm{T}}\}, \tag{7}$$

$$\mathbf{f}_m^{\mathrm{T}} \equiv \{\mathbf{f}_{m11}^{\mathrm{T}} \;\; \mathbf{f}_{m12}^{\mathrm{T}} \;\; \cdots \;\; \mathbf{f}_{m1n}^{\mathrm{T}} \;\; \mathbf{f}_{m21}^{\mathrm{T}} \;\; \mathbf{f}_{m22}^{\mathrm{T}} \;\; \cdots \;\; \mathbf{f}_{m2n}^{\mathrm{T}}\}, \tag{8}$$

where $\mathbf{v}_{m1j}$, $\mathbf{f}_{m1j}$ represent the velocity junction vector and the force junction vector at the source junction for the jth mount and $\mathbf{v}_{m2j}$, $\mathbf{f}_{m2j}$ represent the velocity junction vector and the force junction vector at the receiver junction for the jth mount.

The dynamics of the source and the receiver are studied using a mobility matrix approach so that their velocity and force vectors can be written in the form

$$\mathbf{v}_s = \mathbf{M}_{s1}\mathbf{f}_{s2} + \mathbf{M}_{s2}\mathbf{q}_p, \qquad \mathbf{v}_r = \mathbf{M}_{r1}\mathbf{f}_r + \mathbf{M}_{r2}\mathbf{q}_f, \tag{9, 10}$$

where $\mathbf{M}_{s1}$, $\mathbf{M}_{s2}$ and $\mathbf{M}_{r1}$, $\mathbf{M}_{r2}$ are mobility matrices, respectively, of the source and the receiver structures and $\mathbf{q}_p$, $\mathbf{q}_f$ are the primary excitation vector and the flanking excitation vectors

$$\mathbf{q}_p^{\mathrm{T}} = \{\mathbf{q}_{p1}^{\mathrm{T}} \;\; \mathbf{q}_{p2}^{\mathrm{T}} \;\; \cdots \;\; \mathbf{q}_{pN}^{\mathrm{T}}\}, \qquad \mathbf{q}_f^{\mathrm{T}} = \{\mathbf{q}_{f1}^{\mathrm{T}} \;\; \mathbf{q}_{f2}^{\mathrm{T}} \;\; \cdots \;\; \mathbf{q}_{fM}^{\mathrm{T}}\}, \tag{11, 12}$$

with

$$\mathbf{q}_{pj}^{\mathrm{T}} = \{F_{xj} \;\; F_{yj} \;\; F_{zj} \;\; T_{xj} \;\; T_{yj} \;\; T_{zj}\}, \qquad \mathbf{q}_{fi}^{\mathrm{T}} = \{F_{xj} \;\; F_{yj} \;\; F_{zj} \;\; T_{xj} \;\; T_{yj} \;\; T_{zj}\}, \tag{13, 14}$$

where F_{xj}, F_{yj}, F_{zj} are the complex external forces in the x, y and z directions and T_{xj}, T_{yj}, T_{zj} are the complex external moments referred, respectively, to the x-, y- and z-axes acting at position P_j of the source or receiver structures respectively.

The flanking excitation acting on the receiver $\mathbf{q}_f$ could be due to a subsystem connected with it or to a flanking path connecting the source with the receiver. The dynamics of the mounting system are expressed using an impedance matrix approach

$$\mathbf{f}_m = \mathbf{Z}_m\mathbf{v}_m + \mathbf{V}_m\mathbf{q}_s, \tag{15}$$

where $\mathbf{Z}_m$ is the impedance matrix of the mounting system which relates the linear and angular velocities at each end of the mounts to the forces and moments at each end of the mounts as well. $\mathbf{V}_m$ is the excitation matrix which gives the forces and moments at each end of the mounts due to the control excitations terms which are grouped in the $\mathbf{q}_s$ vector:

$$\mathbf{q}_s^{\mathrm{T}} = \{\mathbf{q}_{s1}^{\mathrm{T}} \;\; \mathbf{q}_{s2}^{\mathrm{T}} \;\; \cdots \;\; \mathbf{q}_{sn}^{\mathrm{T}}\}, \tag{16}$$

where

$$\mathbf{q}_{sj}^{\mathrm{T}} = \{F_{sxj} \;\; F_{syj} \;\; F_{szj} \;\; T_{sxj} \;\; T_{syj} \;\; T_{szj}\} \tag{17}$$

and F_{sxj}, F_{syj}, F_{szj} are the complex control forces in x, y and z directions, while T_{sxj}, T_{syj}, T_{szj} are the complex control torques with reference to the x-, y- and z-axes applied at the P_j mount position. The source and receiver equations (9) and (10) can be grouped together into one equation:

$$\mathbf{v}_{sr} = \mathbf{M}_{sr1}\mathbf{f}_{sr} + \mathbf{M}_{sr2}\mathbf{q}_{pf}, \tag{18}$$

where the mobility matrices and the excitation vector have the form

$$\mathbf{M}_{sr1} = \begin{bmatrix} \mathbf{M}_{s1} & \mathbf{0} \\ \mathbf{0} & \mathbf{M}_{r1} \end{bmatrix}, \qquad \mathbf{M}_{sr2} = \begin{bmatrix} \mathbf{M}_{s2} & \mathbf{0} \\ \mathbf{0} & \mathbf{M}_{r2} \end{bmatrix}, \qquad \mathbf{q}_{pf} = \begin{Bmatrix} \mathbf{q}_p \\ \mathbf{q}_f \end{Bmatrix} \tag{19–21}$$

and the junctions *velocity* and *force vectors* are given by

$$\mathbf{v}_{sr} \equiv \begin{Bmatrix} \mathbf{v}_s \\ \mathbf{v}_r \end{Bmatrix}, \qquad \mathbf{f}_{sr} \equiv \begin{Bmatrix} \mathbf{f}_s \\ \mathbf{f}_r \end{Bmatrix}, \tag{22, 23}$$

where $\mathbf{v}_{sr}$ and $\mathbf{f}_{sr}$ are called, respectively, *source–receiver velocity vector* and *source–receiver force vector*. The source receiver vectors are related to the analogous mounting system vectors by a *transformation matrix* $\mathbf{T}$ in such a way as to satisfy the compatibility condition (for the velocity vectors) and the equilibrium principle (for the force vectors) at each junction

$$\mathbf{v}_m = \mathbf{T}\mathbf{v}_{sr}, \qquad \mathbf{f}_m + \mathbf{T}\mathbf{f}_{sr} = 0. \tag{24, 25}$$

Using these two relations, equations (18) and (15) can be related in such a way as to find the source–receiver velocity vector or the source–receiver force vector as a function of the primary-flanking and secondary excitation vectors:

$$\mathbf{v}_{sr} = \mathbf{Q}_{pv}\mathbf{q}_{pf} + \mathbf{Q}_{sv}\mathbf{q}_s, \qquad \mathbf{f}_{sr} = \mathbf{Q}_{pf}\mathbf{q}_{pf} + \mathbf{Q}_{sf}\mathbf{q}_s, \tag{26, 27}$$

where

$$\mathbf{Q}_{pv} = (\mathbf{I} + \mathbf{M}_{sr1}\mathbf{T}^{-1}\mathbf{Z}_{m1}\mathbf{T})^{-1}\mathbf{M}_{sr2}, \tag{28}$$

$$\mathbf{Q}_{sv} = -(\mathbf{I} + \mathbf{M}_{sr1}\mathbf{T}^{-1}\mathbf{Z}_{m1}\mathbf{T})^{-1}\mathbf{M}_{sr1}\mathbf{T}^{-1}\mathbf{Z}_{m2}, \tag{29}$$

$$\mathbf{Q}_{pf} = -\mathbf{T}^{-1}\mathbf{Z}_{m1}\mathbf{T}(\mathbf{I} + \mathbf{M}_{sr1}\mathbf{T}^{-1}\mathbf{Z}_{m1}\mathbf{T})^{-1}\mathbf{M}_{sr2}, \tag{30}$$

$$\mathbf{Q}_{sf} = \mathbf{T}^{-1}\mathbf{Z}_{m1}\mathbf{T}(\mathbf{I} + \mathbf{M}_{sr1}\mathbf{T}^{-1}\mathbf{Z}_{m1}\mathbf{T})^{-1}\mathbf{M}_{sr1}\mathbf{T}^{-1}\mathbf{Z}_{m2} - \mathbf{T}^{-1}\mathbf{Z}_{m2}. \tag{31}$$

With this model the vibration transmission at each junction is characterized by both kinematic (linear and angular velocities) and dynamic (forces and moments) parameters such that two types of problem arise. First, it is impossible to directly compare the vibration transmission associated with angular velocity and linear velocity or associated with moment and force and second, the standard approach of using either only velocities or only forces to represent the vibrations of the system does not give sufficient information about the effective vibration transmission. Goyder and White [20] have suggested that these two problems can be overcome in the case of isolation of vibration transmission from a rigid source to a flexible receiver by representing the vibration transmission in terms of total structural power transmitted to the receiver. This single parameter accounts for the vibration contribution of all six kinematic and six dynamic parameters at the junctions between the source and receiver structure. This approach has been used in other studies [21–26]. The model used in this study allows this approach to be extended to a multiple mount and multiple d.o.f.s complete isolation system [27]. In fact, using equations (26) and (27) it is possible to express the *time-averaged total power* transmitted to the receiver system in terms of the primary vector and the control vector by using the following equation:

$$P = 1/2\,\mathrm{Re}\{\mathbf{f}_r^{\mathrm{H}}\mathbf{v}_r\}, \tag{32}$$

where $\mathbf{f}_r$ and $\mathbf{v}_r$ represent, respectively, the force and velocity at the receiver structure.

Because the ultimate aim of the study carried out is related to isolation of structure-borne noise transmission it has been preferred to represent the vibration of the receiver structure in terms of its kinetic energy associated only to the bending wave motion which causes the sound radiation. The kinetic energy related to the bending motion of a thin bi-dimensional structure is given by the following relation:

$$K = \int_S \rho h |\dot{w}(s, t)|^2 \, \mathrm{d}S, \tag{33}$$

where ρ is the density of the material, S is the area of the structure and $h(s, t)$, $\dot{w}(s, t)$ are, respectively, the thickness and the out-of-plane velocity at position (s, t) of the structure.

3. CONTROL STRATEGIES

All of the active control strategies considered in the study summarized here can be expressed in terms of a quadratic cost function which is minimized and this can always be written in the form [28]

$$J = \mathbf{q}_s^{\mathrm{H}} \mathbf{A} \mathbf{q}_s + \mathbf{q}_s^{\mathrm{H}} \mathbf{b} + \mathbf{b}^{\mathrm{H}} \mathbf{q}_s + c. \tag{34}$$

The control source that minimizes this quadratic equation is given by [28]

$$\mathbf{q}_{s0} = -\mathbf{A}^{-1} \mathbf{b}. \tag{35}$$

The control strategy of (1) *minimizing total power transmitted by the source to the receiver* was assumed as a reference for assessing the efficacy of the cost functions studied which are (2) the *cancellation of out-of-plane input velocities to the receiver* and (3) the *cancellation of out-of-plane input forces to the receiver*. In this paper, these three control strategies will be referred to as: (1) *total power* minimization (J_p), (2) *velocity* cancellation (J_v) and (3) *force* cancellation (J_f). When the total power is minimized the cost function is

$$J_p = \frac{1}{2} \mathrm{Re}(\mathbf{f}_r^{\mathrm{H}} \mathbf{v}_r) = \frac{1}{4} (\mathbf{f}_r^{\mathrm{H}} \mathbf{v}_r + \mathbf{v}_r^{\mathrm{H}} \mathbf{f}_r), \tag{36}$$

where the receiver velocities and forces parameters at the receiver junctions are given by the two following equations $\mathbf{v}_r = \mathbf{R}_{r1} \mathbf{v}_{sr}$ and $\mathbf{f}_r = \mathbf{R}_{r1} \mathbf{f}_{sr}$ where $\mathbf{R}_{r1} = [\mathbf{0}_{t \times t} \ \mathbf{I}_{t \times t}]$ and $\mathbf{0}_{t \times t}$, $\mathbf{I}_{t \times t}$ are, respectively, a zero matrix and a unit matrix, t is the dimension of the source and receiver vectors. The two matrices in the quadratic form of equation (34) are then needed

$$\mathbf{A}_p = \tfrac{1}{4} (\mathbf{Q}_{sf}^{\mathrm{H}} \mathbf{R}_{r1}^{\mathrm{T}} \mathbf{R}_{r1} \mathbf{Q}_{sv} + \mathbf{Q}_{sv}^{\mathrm{H}} \mathbf{R}_{r1}^{\mathrm{T}} \mathbf{R}_{r1} \mathbf{Q}_{sf}), \quad \mathbf{b}_p = \tfrac{1}{4} (\mathbf{Q}_{sf}^{\mathrm{H}} \mathbf{R}_{r1}^{\mathrm{T}} \mathbf{R}_{r1} \mathbf{Q}_{pv} \mathbf{q}_{pf} + \mathbf{Q}_{sv}^{\mathrm{H}} \mathbf{R}_{r1}^{\mathrm{T}} \mathbf{R}_{r1} \mathbf{Q}_{pf} \mathbf{q}_{pf}). \tag{37, 38}$$

When velocity cancellation is implemented then the cost function has the form

$$J_v = \mathbf{v}_r^{\mathrm{H}} \mathbf{v}_r \tag{39}$$

and the velocity vector $\mathbf{v}_r$ is obtained with the following equation $\mathbf{v}_r = \mathbf{R}_{r2} \mathbf{v}_{sr}$ with $\mathbf{R}_{r1} = [\mathbf{0}_{t \times t} \ \mathbf{H}_{t \times t}]$ and $\mathbf{H}_{t \times t}$ is a zero matrix with diagonal unit terms in correspondence of the row/column related to the z-axis. The two matrices in equation (34) are then given by

$$\mathbf{A}_v = \mathbf{Q}_{sv}^{\mathrm{H}} \mathbf{R}_{r2}^{\mathrm{T}} \mathbf{R}_{r2} \mathbf{Q}_{sv}, \qquad \mathbf{b}_v = \mathbf{Q}_{sv}^{\mathrm{H}} \mathbf{R}_{r2}^{\mathrm{T}} \mathbf{R}_{r2} \mathbf{Q}_{pv} \mathbf{q}_{pf}. \tag{40, 41}$$

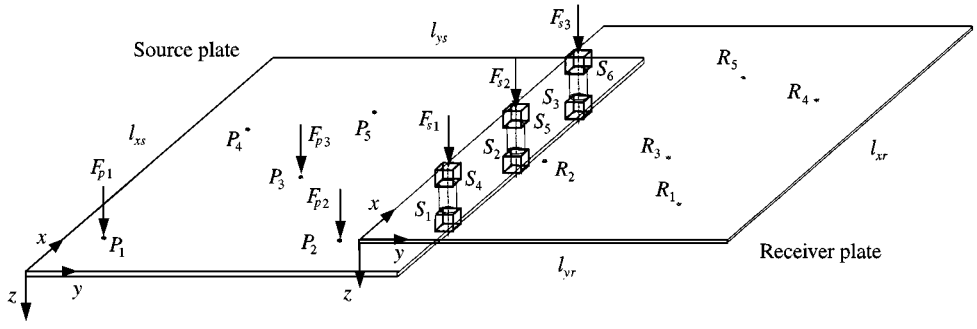

Figure 2. The system studied.

When force cancellation is implemented then the cost function has the form

$$J_f = \mathbf{f}_r^{\mathrm{H}} \mathbf{f}_r \tag{42}$$

and the force vector $\mathbf{f}_r$ is obtained with the following equation $\mathbf{f}_r = \mathbf{R}_{r2}\mathbf{f}_{sr}$. The two matrices in equation (34) are then given by

$$\mathbf{A}_f = \mathbf{Q}_{sf}^{\mathrm{H}} \mathbf{R}_{r2}^{\mathrm{T}} \mathbf{R}_{r2} \mathbf{Q}_{sf}, \qquad \mathbf{b}_f = \mathbf{Q}_{sf}^{\mathrm{H}} \mathbf{R}_{r2}^{\mathrm{T}} \mathbf{R}_{r2} \mathbf{Q}_{pf} \mathbf{q}_{pf}. \tag{43, 44}$$

4. THE SYSTEMS STUDIED

Figure 2 shows the geometry of the system studied. The source and receiver structures are freely suspended aluminium plates having dimensions of $l_{xs} \times l_{ys} = l_{xr} \times l_{yr} = 1{\cdot}2 \times 1{\cdot}0$ m and thickness $t_s = 3$ mm, $t_r = 1{\cdot}5$ mm. The physical properties of the two plates are assumed to be: density $\rho_s = \rho_r = 2796\ \mathrm{kg/m^3}$, Young's modulus of elasticity $E_s = E_r = 7{\cdot}24 \times 10^{10}\ \mathrm{N/m^2}$, the Poisson ratio $\nu_s = \nu_r = 0{\cdot}3$, and loss factor $\eta_s = \eta_r = 0{\cdot}01$. The three mounts are modelled as cylinders of soft rubber with either a single sky hook control force acting at the top end of the mounts or two equal reactive control forces acting at each end of the mounts. The diameter and the height of the suspensions are, respectively, $\phi_m = 15$ mm and $h_m = 15$ mm while the physical properties of the rubber are: density $\rho_m = 1078\ \mathrm{kg/m^3}$, Young's modulus of elasticity $E_m = 1{\cdot}5 \times 10^6\ \mathrm{N/m^2}$, the Poisson ratio $\nu_m = 0{\cdot}49$ and the loss factor $\eta_m = 0{\cdot}05$. Also, a stiffer mounting system has been modelled by assuming the mounts as cylinders of aluminium with physical properties: $\rho_m = 2796\ \mathrm{kg/m^3}$, $E_m = 7{\cdot}24 \times 10^{10}\ \mathrm{N/m^2}$, $\nu_m = 0{\cdot}3$ and $\eta_m = 0{\cdot}01$. The effects generated by the components used to connect the mounting system to the plates and to connect force and velocity sensors at the top of the mounts has been modelled as a pair of rectangular parallelepiped block masses connected at each end of the mounts. The dimensions and weight of the masses attached to the top side of the mounts are: $d_{xt} \times d_{yt} \times d_{zt} = 12 \times 12 \times 24$ mm, $W_t = 9{\cdot}8 \times 10^{-3}$ kg while the dimensions and weight of the masses attached to the bottom side of the mounts are: $d_{xb} \times d_{yb} \times d_{zb} = 8 \times 8 \times 8$ mm, $W_b = 3{\cdot}1 \times 10^{-3}$ kg.

The source and receiver plates are assumed to be distributed elements and the model considers only the effect of bending waves. In-plane shear and longitudinal waves are neglected since their sound radiation effect is negligible and their coupling to the bending motion of the plate due to the mounting system is also negligible. The mounts are modelled as distributed systems on which longitudinal and flexural waves can propagate.

TABLE 1

Mount junction positions at the source plate

	x(m)	y(m)
S_1	0·2	0·991
S_2	0·6	0·991
S_3	1	0·991

TABLE 2

Mount junction positions at the receiver plate

	x(m)	y(m)
S_4	0·2	0·009
S_5	0·6	0·009
S_6	1	0·009

Therefore, the matrix model described in section 2 has been used by considering only 3 d.o.f.s at the mount junctions and at the excitation positions. Appendices A and B describe the formulation of the driving point and transfer mobility or impedance terms for the plate and mount systems respectively. The reduction from 6 to 3 d.o.f.s is not trivial and, as discussed in Appendix B, the equations of the driving point and transfer impedances for the mount systems differs in the two cases.

The velocity and force junction vectors of equations (1,2) have therefore been assumed as follows:

$$\mathbf{v}_j^{\mathrm{T}} \equiv \{\dot{w}_j \;\; \dot{\theta}_{xj} \;\; \dot{\theta}_{yj}\}, \qquad \mathbf{f}_j^{\mathrm{T}} \equiv \{N_{zj} \;\; M_{xj} \;\; M_{yj}\}, \tag{45,46}$$

where $\dot{w}_j$ is the linear velocity in the z direction, $\dot{\theta}_{xj}$ and $\dot{\theta}_{yj}$ are the angular velocities referred, respectively, to the x- and y-axis, N_{zj} is the force in the z direction and M_{xj}, M_{yj} are the moments referred, respectively, to the x- and y-axis. The positions of the mount junctions at the source (S_1, S_2, S_3) and receiver (S_4, S_5, S_6) plates are given in Tables 1 and 2.

Three primary excitation positions have been selected in such a way as to coincide with the first three monitoring positions P_1, P_2, P_3 of the source plate. The jth excitation vector is composed of three components: an out-of-plane force in the z direction F_{zj} and two torques in the x and y directions T_{xj} and T_{yj} so that

$$\mathbf{q}_{pj}^{\mathrm{T}} \equiv \{F_{zj} \;\; T_{xj} \;\; T_{yj}\}. \tag{47}$$

Finally, because only sky hook or reactive axial control forces have been considered the control vector $\mathbf{q}_{sj}$ of equation (17) assumes the following form

$$\mathbf{q}_{sj}^{\mathrm{T}} \equiv F_{szj}. \tag{48}$$

The monitoring positions of the source $P_1, P_2, \ldots, P_5$ and receiver $R_1, R_2, \ldots, R_5$ plates are summarized in Tables 3 and 4.

TABLE 3

Monitoring positions at the source plate

	x(m)	y(m)
P_1	0·26	0·175
P_2	0·26	0·82
P_3	0·55	0·475
P_4	0·77	0·195
P_5	0·96	0·43

TABLE 4

Monitoring positions at the receiver plate

	x(m)	y(m)
R_1	0·26	0·64
R_2	0·42	0·18
R_3	0·55	0·525
R_4	0·77	0·805
R_5	0·96	0·57

These positions are called monitoring positions since, for practical purposes, they have been chosen to represent the vibration levels of the source and receiver plates by an estimate of the plates kinetic energy associated with the bending motion which is given by the sum of the squared values of the out-of-plane velocities at the monitoring positions of the plates:

$$K_{Es} = \mathbf{v}_P^{\mathrm{H}} \mathbf{v}_P, \qquad K_{Er} = \mathbf{v}_R^{\mathrm{H}} \mathbf{v}_R, \tag{49, 50}$$

where

$$\mathbf{v}_P^{\mathrm{T}} = \{\dot{w}_{P1} \;\; \dot{w}_{P2} \;\; \dot{w}_{P3} \;\; \dot{w}_{P4} \;\; \dot{w}_{P5}\}, \qquad \mathbf{v}_R^{\mathrm{T}} = \{\dot{w}_{R1} \;\; \dot{w}_{R2} \;\; \dot{w}_{R3} \;\; \dot{w}_{R4} \;\; \dot{w}_{R5}\}. \tag{51, 52}$$

The estimate of the source and receiver kinetic energy has been used to compare and validate the matrix model used in this study with experimental measurements taken on a similar system.

No flanking excitation was considered to be acting on the receiver plate so that the matrix equations (9) and (10) assume the following forms:

$$\begin{Bmatrix} \mathbf{v}_{S1} \\ \mathbf{v}_{S2} \\ \mathbf{v}_{S3} \end{Bmatrix} = \begin{bmatrix} \mathbf{M}_{S1S1} & \mathbf{M}_{S1S2} & \mathbf{M}_{S1S3} \\ \mathbf{M}_{S2S1} & \mathbf{M}_{S2S2} & \mathbf{M}_{S2S3} \\ \mathbf{M}_{S3S1} & \mathbf{M}_{S3S2} & \mathbf{M}_{S3S3} \end{bmatrix} \begin{Bmatrix} \mathbf{f}_{S1} \\ \mathbf{f}_{S2} \\ \mathbf{f}_{S3} \end{Bmatrix} + \begin{bmatrix} \mathbf{M}_{S1P1} & \mathbf{M}_{S1P2} & \mathbf{M}_{S1P3} \\ \mathbf{M}_{S2P1} & \mathbf{M}_{S2P2} & \mathbf{M}_{S2P3} \\ \mathbf{M}_{S3P1} & \mathbf{M}_{S3P2} & \mathbf{M}_{S3P3} \end{bmatrix} \begin{Bmatrix} \mathbf{q}_{P1} \\ \mathbf{q}_{P2} \\ \mathbf{q}_{P3} \end{Bmatrix}, \tag{53}$$

$$\begin{Bmatrix} \mathbf{v}_{S4} \\ \mathbf{v}_{S5} \\ \mathbf{v}_{S6} \end{Bmatrix} = \begin{bmatrix} \mathbf{M}_{S4S4} & \mathbf{M}_{S4S5} & \mathbf{M}_{S4S6} \\ \mathbf{M}_{S5S4} & \mathbf{M}_{S5S5} & \mathbf{M}_{S5S6} \\ \mathbf{M}_{S6S4} & \mathbf{M}_{S6S5} & \mathbf{M}_{S6S6} \end{bmatrix} \begin{Bmatrix} \mathbf{f}_{S4} \\ \mathbf{f}_{S5} \\ \mathbf{f}_{S6} \end{Bmatrix}. \tag{54}$$

Because the mounts are all the same, the impedance equation (15) assumes a simplified form which is given by the following two equations in the case of a reactive or an inertial control force scheme respectively:

$$\begin{Bmatrix} \mathbf{f}_{S1} \\ \mathbf{f}_{S2} \\ \mathbf{f}_{S3} \\ \mathbf{f}_{S4} \\ \mathbf{f}_{S5} \\ \mathbf{f}_{S6} \end{Bmatrix} = \begin{bmatrix} \mathbf{Z}_{11} & \mathbf{0} & \mathbf{0} & \mathbf{Z}_{12} & \mathbf{0} & \mathbf{0} \\ \mathbf{0} & \mathbf{Z}_{11} & \mathbf{0} & \mathbf{0} & \mathbf{Z}_{12} & \mathbf{0} \\ \mathbf{0} & \mathbf{0} & \mathbf{Z}_{11} & \mathbf{0} & \mathbf{0} & \mathbf{Z}_{12} \\ \mathbf{Z}_{21} & \mathbf{0} & \mathbf{0} & \mathbf{Z}_{22} & \mathbf{0} & \mathbf{0} \\ \mathbf{0} & \mathbf{Z}_{21} & \mathbf{0} & \mathbf{0} & \mathbf{Z}_{22} & \mathbf{0} \\ \mathbf{0} & \mathbf{0} & \mathbf{Z}_{21} & \mathbf{0} & \mathbf{0} & \mathbf{Z}_{22} \end{bmatrix} \begin{Bmatrix} \mathbf{v}_{S1} \\ \mathbf{v}_{S2} \\ \mathbf{v}_{S3} \\ \mathbf{v}_{S4} \\ \mathbf{v}_{S5} \\ \mathbf{v}_{S6} \end{Bmatrix} + \begin{bmatrix} -\mathbf{V}_1 & \mathbf{0} & \mathbf{0} \\ \mathbf{0} & -\mathbf{V}_1 & \mathbf{0} \\ \mathbf{0} & \mathbf{0} & -\mathbf{V}_1 \\ \mathbf{V}_1 & \mathbf{0} & \mathbf{0} \\ \mathbf{0} & \mathbf{V}_1 & \mathbf{0} \\ \mathbf{0} & \mathbf{0} & \mathbf{V}_1 \end{bmatrix} \begin{Bmatrix} \mathbf{q}_{s1} \\ \mathbf{q}_{s2} \\ \mathbf{q}_{s3} \end{Bmatrix}, \tag{55}$$

$$\begin{Bmatrix} \mathbf{f}_{S1} \\ \mathbf{f}_{S2} \\ \mathbf{f}_{S3} \\ \mathbf{f}_{S4} \\ \mathbf{f}_{S5} \\ \mathbf{f}_{S6} \end{Bmatrix} = \begin{bmatrix} \mathbf{Z}_{11} & \mathbf{0} & \mathbf{0} & \mathbf{Z}_{12} & \mathbf{0} & \mathbf{0} \\ \mathbf{0} & \mathbf{Z}_{11} & \mathbf{0} & \mathbf{0} & \mathbf{Z}_{12} & \mathbf{0} \\ \mathbf{0} & \mathbf{0} & \mathbf{Z}_{11} & \mathbf{0} & \mathbf{0} & \mathbf{Z}_{12} \\ \mathbf{Z}_{21} & \mathbf{0} & \mathbf{0} & \mathbf{Z}_{22} & \mathbf{0} & \mathbf{0} \\ \mathbf{0} & \mathbf{Z}_{21} & \mathbf{0} & \mathbf{0} & \mathbf{Z}_{22} & \mathbf{0} \\ \mathbf{0} & \mathbf{0} & \mathbf{Z}_{21} & \mathbf{0} & \mathbf{0} & \mathbf{Z}_{22} \end{bmatrix} \begin{Bmatrix} \mathbf{v}_{S1} \\ \mathbf{v}_{S2} \\ \mathbf{v}_{S3} \\ \mathbf{v}_{S4} \\ \mathbf{v}_{S5} \\ \mathbf{v}_{S6} \end{Bmatrix} + \begin{bmatrix} \mathbf{0} & \mathbf{0} & \mathbf{0} \\ \mathbf{0} & \mathbf{0} & \mathbf{0} \\ \mathbf{0} & \mathbf{0} & \mathbf{0} \\ \mathbf{V}_1 & \mathbf{0} & \mathbf{0} \\ \mathbf{0} & \mathbf{V}_1 & \mathbf{0} \\ \mathbf{0} & \mathbf{0} & \mathbf{V}_1 \end{bmatrix} \begin{Bmatrix} \mathbf{q}_{s1} \\ \mathbf{q}_{s2} \\ \mathbf{q}_{s3} \end{Bmatrix}. \tag{56}$$

Expressions for the mobility $\mathbf{M}_{ij}$, impedance $\mathbf{Z}_{ij}$ and excitation matrix $\mathbf{V}_1$ matrices are given in Appendices A and B. Once the force parameters at the mounting junction positions are calculated with equation (27) it is possible to derive the out-of-plane velocities at the monitoring positions of the source and receiver plate with the following two relations:

$$\begin{Bmatrix} \dot{w}_{P1} \\ \dot{w}_{P2} \\ \dot{w}_{P3} \\ \dot{w}_{P4} \\ \dot{w}_{P5} \end{Bmatrix} = \begin{bmatrix} \mathbf{M}_{P1S1} & \mathbf{M}_{P1S2} & \mathbf{M}_{P1S3} \\ \mathbf{M}_{P2S1} & \mathbf{M}_{P2S2} & \mathbf{M}_{P3S3} \\ \mathbf{M}_{P3S1} & \mathbf{M}_{P3S2} & \mathbf{M}_{P3S3} \\ \mathbf{M}_{P4S1} & \mathbf{M}_{P4S2} & \mathbf{M}_{P4S3} \\ \mathbf{M}_{P5S1} & \mathbf{M}_{P5S2} & \mathbf{M}_{P5S3} \end{bmatrix} \begin{Bmatrix} \mathbf{f}_{S1} \\ \mathbf{f}_{S2} \\ \mathbf{f}_{S3} \end{Bmatrix}, \quad \begin{Bmatrix} \dot{w}_{R1} \\ \dot{w}_{R2} \\ \dot{w}_{R3} \\ \dot{w}_{R4} \\ \dot{w}_{R5} \end{Bmatrix} = \begin{bmatrix} \mathbf{M}_{R1S4} & \mathbf{M}_{R1S5} & \mathbf{M}_{R1S6} \\ \mathbf{M}_{R2S4} & \mathbf{M}_{R2S5} & \mathbf{M}_{R3S6} \\ \mathbf{M}_{R3S4} & \mathbf{M}_{R3S5} & \mathbf{M}_{R3S6} \\ \mathbf{M}_{R4S4} & \mathbf{M}_{R4S5} & \mathbf{M}_{R4S6} \\ \mathbf{M}_{R5S4} & \mathbf{M}_{R5S5} & \mathbf{M}_{R5S6} \end{bmatrix} \begin{Bmatrix} \mathbf{f}_{S4} \\ \mathbf{f}_{S5} \\ \mathbf{f}_{S6} \end{Bmatrix}, \tag{57, 58}$$

5. CONTROL EFFECTIVENESS OF THE ISOLATOR SYSTEM

In this section, the results obtained for the simulations of isolator system with the three rubber mounts shown in Figure 2 are described. Two types of secondary sources are considered in detail: first, a sky-hook control force and second, a reactive control force. The sky-hook control force can be generated by an inertial actuator placed at the top of the mount while the reactive control force can be obtained by an actuator placed in parallel with the passive element of the mount. For each case two plots have been considered: the first (Figure 3) shows the estimate of kinetic energy at the source and receiver panels calculated with equations (49) and (50), when a harmonic unit primary force F_{P3} is exciting

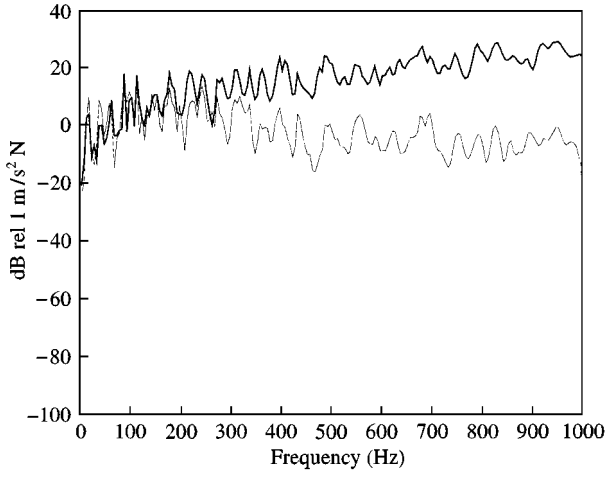

Figure 3. Estimate of the source K_{Es} (———) and receiver K_{Er} (——) kinetic energy when the primary force F_{p3} is exciting the two-panel system with three-rubber mounts with block masses.

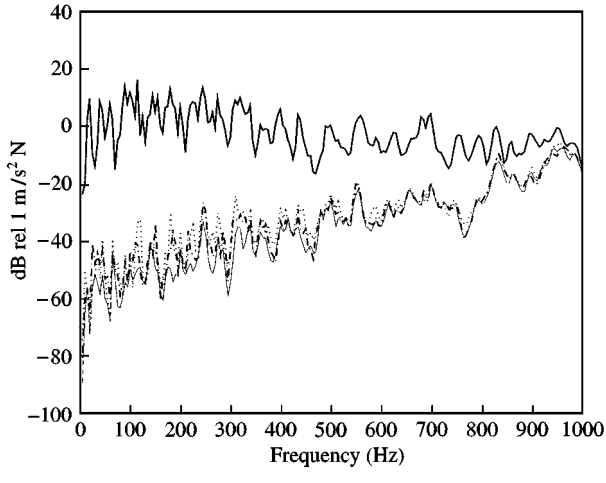

Figure 4. Estimate of the receiver K_{Er} kinetic energy when the primary force F_{p3} is exciting the two panel system with three rubber mounts with block masses and a *sky-hook* control force. ———, without control; ——, when total power is minimized; ·····, when forces are cancelled; – · – · – · – when velocities are cancelled.

the system and with no active control, while the second (either Figure 4 or 5) shows the estimate of kinetic energy of the receiver panels when a harmonic unit primary force F_{P3} is exciting the system, and the secondary forces are set to implement the power minimization, velocity and force cancellation cost functions described in section 3.

Considering the passive behaviour of the system, as shown in Figure 3. It can be seen that the three rubber mounts produce good passive isolation effects above 300 Hz and the ratio of the kinematic energy in the source and receiver panel can reach a level of about 30 dB at 1 kHz.

Figures 4 and 5 show the effects of the different active control strategies. In general, the three control strategies under study, power minimization and force or velocity cancellation,

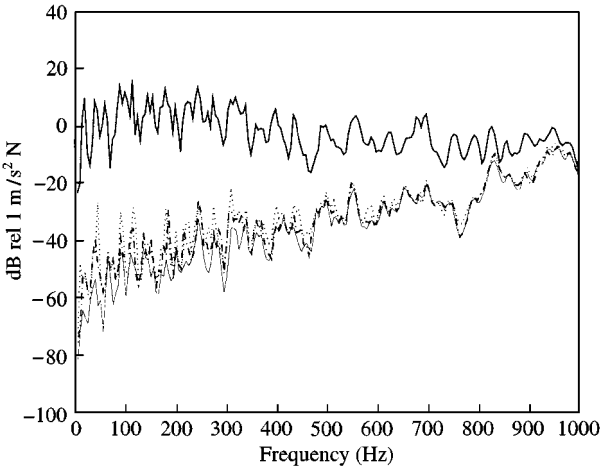

Figure 5. Estimate of the receiver K_{Er} kinetic energy when the primary force F_{p3} is exciting the two-panel system with three rubber mounts with block masses and a pair of *reactive* control forces. ———, without control; ——, when total power is minimised; ·····, when forces are cancelled; –·–·–·–· when velocities are cancelled.

have given similar control effects. Comparing the results of Figure 4 with those of Figure 5, no major differences in the control effectiveness are shown when the reactive actuators are used in place of the inertial actuators. Both Figures 4 and 5 show that the control effectiveness decreases as the frequency rises. This is because, at low frequencies, the vibration of the source plate is mainly transmitted via the axial d.o.f. of the mount. In contrast, at higher frequencies both the axial and angular d.o.f. contribute to the vibration transmission. The two types of active mounts considered in this paper have only axial control forces that can efficiently control the axial vibration transmission but cannot control the vibration transmission through the angular d.o.f. at higher frequencies. An active mount with control actuators generating both the axial control force and two control moments in x and y directions would certainly increase the active isolation at high frequencies. The multiple mount system of Figure 2 can be regarded as a system capable of generating control moments in y direction by driving out of phase the axial control forces of each couple of mounts. A triangular configuration of the three mounts would allow the generation of moments in both x and y directions. In any case, this effect is given only for low frequencies where the distance between the mounts is higher than the bending wave length in the plate [5,29,30].

6. EFFECTS OF THE BLOCK MASSES AND MOUNTING SYSTEM STIFFNESS

The simulations carried out for the three-mount isolators have shown that good passive isolation is obtained when block masses of 9·8 and 3·1 gm are applied at each end of the mounts. In this section, the relation between the weight of these masses and the effectiveness of the isolation has been assessed by considering the three rubber-mount isolator system with sky-hook control forces shown in Figure 2 when the velocity control strategy is implemented and the masses listed in Table 5 are applied to each end of the three mounts.

The conclusion that can be drawn from Figure 6 is that as the weight of the block masses rises, both the passive and active isolation tend to increase at higher frequencies. The additional passive isolation is effective at frequencies above about 250 Hz and tends to grow

TABLE 5

Weights of the top and bottom masses

Case	W_T(kg)	W_B(kg)
a	0	0
b	$1{\cdot}5 \times 10^{-3}$	5×10^{-3}
c	3.0×10^{-3}	10×10^{-3}
d	6.0×10^{-3}	20×10^{-3}
e	9.0×10^{-3}	30×10^{-3}
f	12.0×10^{-3}	40×10^{-3}

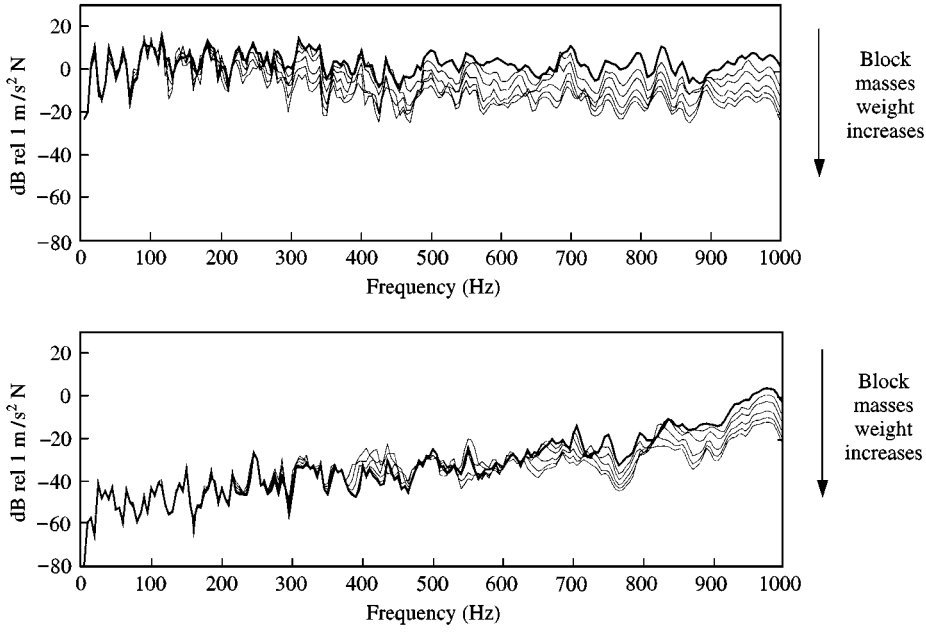

Figure 6. Estimate of the receiver K_{Er} kinetic energy before (top plot) and after (bottom plot) active control by means of the velocity control strategy using sky-hook control forces when the primary force F_{p3} is exciting the two panels system, for the block masses shown in Table 5: ——— is case (a).

as the frequency rises. The additional isolation effect due to the block masses with active control is only effective above about 620 Hz and then also tends to grow as the frequency increases. This phenomena is due to the fact that the specific impedance of a block mass rises linearly with frequency. Thus, as the frequency rises, the masses on the receiving junction of each mount tend to block the axial vibration at this point and so improve the passive transmission properties above 250 Hz. This axial vibration is already controlled by the active system, however, and it appears as though in this case the rotary inertia of the block masses enhances the active transmission properties at higher frequencies by decreasing the level of rotational velocity transmitted through the mounts, which otherwise degrades the transmission properties of the active system. Figure 6, bottom plot, shows that between 360 and 440 Hz the trend described above is inverted for the active isolation case so that the isolation is slightly reduced as the weight of the masses increases.

TABLE 6

Stiffness and density of the mounts

Case	E_m(N/m^2)	ρ_m(kg/m^3)
a	$7{\cdot}5 \times 10^4$	648
b	$1{\cdot}5 \times 10^6$	1078
c	$2{\cdot}9 \times 10^7$	1508
d	$4{\cdot}3 \times 10^8$	1938
e	$5{\cdot}8 \times 10^9$	2368
f	$7{\cdot}2 \times 10^{10}$	2798

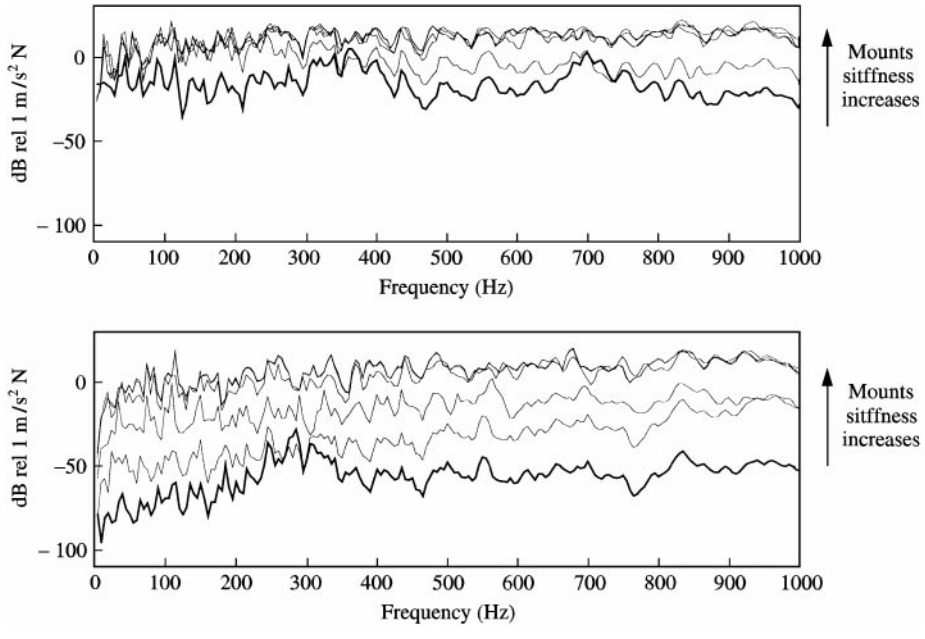

Figure 7. Estimate of the receiver K_{Er} kinetic energy before (top plot) and after (bottom plot) active control by means of the velocity control strategy using sky-hook control forces when the primary force F_{p3} is exciting the two-panel system, for the mount stiffnesses shown in Table 6: ——— is case (a).

The simulations carried out have also shown that the stiffness of the mounts affect both the passive and active isolation. The passive and active isolation when velocity cancellation is implemented has been evaluated with reference to the system with three mounts and sky-hook control forces shown in Figure 2 by considering a set of mounts whose density and stiffness has been chosen between two limiting cases: first (a), a very soft rubber mount and last (f), a relatively stiff aluminium mount as summarized in Table 6. Considering the results shown in Figure 7, it can be concluded that both the passive and active isolation tend to get better as the stiffness and density of the mounts decrease (e.g., as the specific impedance of the mounts decrease). When the impedance of the mounts is relatively small compared to that of the source and receiver plates, then the mounts can be deformed in such a way as to accommodate both the imposed vibration of the source plate and the imposed

constrain of the receiver plate. This phenomena is more effective at higher frequencies since the specific impedance of the mounts decrease linearly with frequency. Also, Figure 7 shows that as the stiffness and density of the mounts increase the benefits of active control vanish so that passive and active isolation give similar results. Thus, even if very large control forces can reduce the axial vibration at the junctions between the mounts and the receiver plate, still there is a large vibration transmission effect via the angular motion of the solid mount.

7. COMPARISON BETWEEN IMM SIMULATIONS AND EXPERIMENTAL RESULTS

The impedance-mobility matrix model IMM described in this paper has been tested by comparing the results it produces with two other types of analysis. First, a matrix analysis which uses measured transfer functions from an experimental arrangement similar to that described above between the primary and control excitation positions and the control positions at the mount junctions and the monitoring positions on the receiver panel denoted MTF, and second, a fully experimental analysis carried out at a set of 24 tones between 110 and 340 Hz, denoted EA. The comparison has been carried out for the two-plate system shown in Figure 2 having either a rubber or aluminium mount with lumped masses at the top and bottom ends and with inertial control actuators acting at the top end of the mounts. The control strategy tested was the cancellation of axial velocities at the top of the mounts. The primary excitation has been chosen at position P_3. Figures 8 and 9 show the estimate of the receiver K_{Er} kinetic energy without active control (upper plots) for the two types of isolator systems. In both cases, rubber and aluminium isolators, very good agreement has been obtained between the three types of predictions without control.

Figures 8 and 9 also show results with active control (lower plots). The comparison between the three types of predictions with active control are generally good. Above 150 Hz the IMM simulations agree quite well with the matrix approach based on measured transfer functions MTF. Below 150 Hz there are some discrepancies between the IMM and the MTF predictions which are probably due to the fact that the experimental transfer functions used by the MTF approach are not reliable below 100 Hz. Also, the bottom plot of Figure 9 shows that when the aluminium isolator is used there is a mismatching of about 10 dB in a frequency range between 520 and 980 Hz between the predictions with the IMM model and those obtained from the MFT method. The method using measured transfer functions, MTF, predicts larger active isolation than that of the analytical model IMM. This could be due to the non-perfect alignment of the mounts in the experimental rig, so that a larger control effectiveness is predicted, since the experimental control system is able to reduce not only the vibration transmission due to axial vibration of the mounts but also the vibration transmission related to the angular vibrations of the mounts.

8. CONCLUSIONS

This paper introduces the theory of an impedance-mobility matrix model used to predict the structural vibration transmission between two plates coupled via an active mounting system. With this model the active and passive isolation effectiveness of different types of mounting systems have been studied; in particular, the case of a three-mount isolator system with inertial actuators applied at the top end of the mounts has been investigated in order to assess the effects generated by the stiffness of the mounts and the effects produced by the rigid elements (block masses) at each end of the mounts.

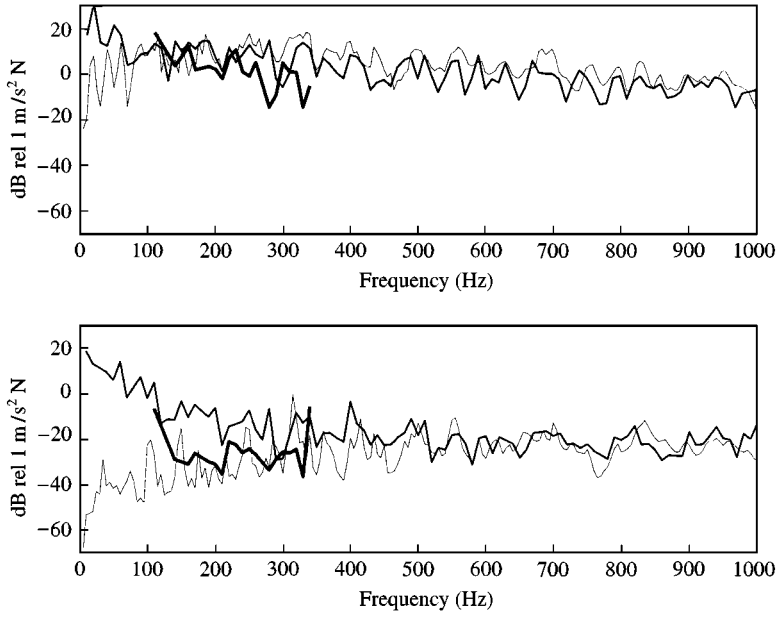

Figure 8. Estimate of the receiver K_{Er} kinetic energy without (top plot) and with (bottom plot) active control of the out-of-plane velocities at the receiver mounts junction when the primary force F_{p3} is exciting the two-panel system with three-rubber mounts having block masses at the ends: ———, measure transfer functions predictions; ——: impedance mobility matrix predictions; ——, experimental analysis predictions.

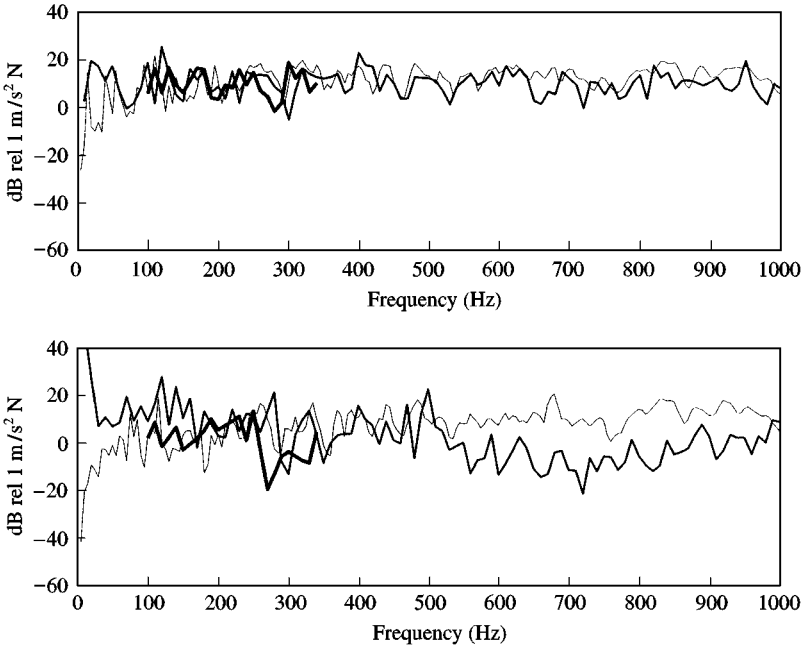

Figure 9. Estimate of the receiver K_{Er} kinetic energy without (top plot) and with (bottom plot) active control of the out-of-plane velocities at the receiver mounts junction when the primary force F_{p3} is exciting the two-panel system with three-aluminium mounts having block masses at the ends: ———, measure transfer functions predictions; ——: impedance mobility matrix predictions; ——, experimental analysis predictions.

Three cost functions have been investigated: first, the minimization of the total structural power transmitted by the source to the receiver; second, the cancellation of out-of-plane input velocities to the receiver and the cancellation of out-of-plane input forces to the receiver.

The main conclusions of the study carried out can be summarized by the following points.

1. The rubber mount isolator provides better passive isolation effects than that with aluminium mounts, as expected.
2. When block masses are applied at each end of the rubber mounts an extra isolation effect is obtained. This effect is negligible when aluminium mounts are used.
3. The three control strategies under study have given similar active control effectiveness in all cases examined.
4. No major differences have been found when the reactive actuators are used in place of the inertial actuators.
5. The presence of block masses mounted at each end of the mounts do not produce significant effects below 620 Hz on the active control performances of both rubber and aluminium mounts.
6. The rubber active isolators give very good active control performance which goes from a maximum of about 60 dB reduction at very low frequency to a minimum of a few dB at about 1 kHz while the active isolator with aluminium mounts gives very poor control performances.

The model described in this paper has been validated with data given by two other methods. First, a matrix method based on measured transfer functions and second, an experimental method which considered real-time active control for tonal excitations.

ACKNOWLEDGMENTS

Part of the work reported here was supported by the Aero-Structures Department at DERA Farnborough, and in particular the support and collaboration of Professor K. Heron and Mr R. Harris is gratefully acknowledged.

REFERENCES

1. C. E. Crede and J. E. Ruzicka 1976 *Shock and Vibration Handbook* (Harris and C. E. Crede editors) New York: McGraw-Hill, chapter 30. Theory of vibration isolation.
2. M. Petyt 1998 *Introduction to Finite Element Vibration Analysis* Cambridge: Cambridge University, second edition.
3. R. H. Lyon and R. G. DeJong 1995 *Theory and Application of Statistical Energy Analysis.* Oxford: Butterworth-Heinemann, second edition.
4. K. H. Heron 1998 *DERA/MSS5/TR*980720, *DERA*, *Farnborough*, *U.K.* Predictive statistical energy analysis and collocated active control.
5. P. Gardonio, S. J. Elliott and R. J. Pinnington 1997 *Journal of Sound and Vibration*, **207**, 61–93. Active isolation of structural vibration on multiple-degree-of-freedom system. Part I: dynamics of the system.
6. E. Skudrzyk 1959 *The Journal of the Acoustical Society of America* **31**, 68–74. Theory of noise and vibration insulation of a system with many resonances.
7. J. C. Snowdon 1961 *Journal of the Acoustical Society of America* **33**, 1466–1475. Reduction of the response to vibration of structures possesing finite mechanical impedance.
8. J. C. Snowdon 1962 *Journal of the Acoustical Society of America* **34**, 54–61. Isolation from vibration with a mounting utilizing low- and high-damping rubberlike materials.
9. S. Rubin 1964 *Transaction of the ASME Journal of Engineering for Industry* **86**, 9–21. Transmission matrices for vibration and their relation to admittance and impedance.

10. J. C. SNOWDON 1965 *Journal of Sound and Vibration* **2**, 175–193. Rubberlike materials, their internal damping and role in vibration isolation.
11. E. E. UNGAR and C. W. DIETRICH 1966 *Journal of Sound and Vibration* **4**, 224–241. High-frequency vibration isolation.
12. S. RUBIN 1967 *Journal of the Acoustical Society of America* **41**, 1171–1179. Mechanical immitance- and transmission-matrix concepts.
13. S. RUBIN 1967 Proceedings of *Aeronautic and Space Engineering and Manufacturing Meeting, Los Angeles*. Mechanical impedance approach to engine vibration transmission into an aircraft fuselage.
14. J. I. SOLIMAN and M. G. HALLAM 1968 *Journal of Sound and Vibration* **8**, 329–351. Vibration isolation between non-rigid machines and non-rigid foundations.
15. J. C. SNOWDON 1971 *Journal of Sound and Vibration* **15**, 307–323. Mechanical four-pole parameters and their application.
16. M. L. MUNJAL 1975 *Journal of Sound and Vibration* **39**, 247–263. A rational synthesis of vibration isolators.
17. B. PETERSSON and J. PLUNT 1982 *Journal of Sound and Vibration* **82**, 517–529. On effective mobilities in the prediction of structure-borne sound transmission between a source structure and a receiving structure. Part I: theoretical background and basic experimental studies.
18. J. H. GORDIS, R. L. BIELAWA and W. G. FLANNELLY 1991 *Journal of Sound and Vibration* **150**, 139–158. A general theory for frequency domain structural synthesis.
19. D. A. SWANSON, L. R. MILLER and M. A. NORRIS 1994 *Journal of Aircraft* **31**, 188–196. Multidimensional mount effectiveness for vibration isolation.
20. H. G. D. GOYDER and R. G. WHITE 1980 *Journal of Sound and Vibration* **68**, 59–75. Vibrational power flow from machines into built-up structures. Part I: introduction and approximate analyses of beam and plate-like foundations.
21. R. J. PINNINGTON and R. G. WHITE 1980 *Journal of Sound and Vibration* **75**, 179–197. Power flow through machine isolators to resonant and non-resonant beams.
22. R. J. PINNINGTIN 1987 *Journal of Sound and Vibration* **118**, 515–530. Vibrational power transmission to a seating of a vibration isolated motor.
23. R. J. PINNINGTON 1990 *Journal of Sound and Vibration* **137**, 117–129. Vibrational power transmission from a finite source beam to an infinite receiver beam via a continuous compliant mount.
24. JIE PAN, JIAQIANG PAN and C. H. HANSEN 1992 *Journal of the Acoustical Society of America* **92**, 895–907. Total power flow from a vibrating rigid body to a thin panel through multiple elastic mounts.
25. J. E. FARSTAD and R. SINGH 1995 *Journal of the Acoustical Society of America* **97**, 2855–2865. Structurally transmitted dynamic power in discretely joined damped component assemblies.
26. T. E. ROOK and R. SINGH 1995 *Journal of the Acoustical Society of America* **97**, 2882–2891. Power flow through multidimensional compliant joints using mobility and modal approaches.
27. P. GARDONIO and S. J. ELLIOTT 1999 *ASME Journal of Vibration and Acoustics* **121**, 482–487. A study of control strategies for the reduction of structural vibration transmission.
28. C. R. FULLER, S. J. ELLIOTT and P. A. NELSON 1997 *Active Control of Vibration*. London: Academic Press.
29. O. BARDOU, P. GARDONIO, S. J. ELLIOTT, and R. J. PINNINGTON 1997 *Journal of Sound and Vibration* **208**, 111–151. Active power minimization and power absorption in a plate with force and momen excitation.
30. P. GARDONIO, S. J. ELLIOTT and R. J. PINNINGTON 1997 *Journal of Sound and Vibration* **207**, 95–121. Active isolation of structural vibration on multiple-degree-of-freedom system. Part II: effectiveness of active control strategies.
31. P. GARDONIO and S. J. ELLIOTT 1998 *Technical Report No* 277, *ISVR, University of Southampton*. Driving point and transfer mobility matrices for thin plates excited in flexure.
32. L. CREMER, M. HECKL and E. E. UNGAR 1988 *Structure-Borne Sound*. Berlin: Springer-Verlag, second edition.
33. G. J. O'HARA 1966 *Journal of the Acoustical Society of America* **41**, 1180–1184. Mechanical impedance and mobility concepts.
34. R. E. D. BISHOP and D. C. JOHNSON 1960 *The Mechanics of Vibration*. Cambridge: The Cambridge University Press.

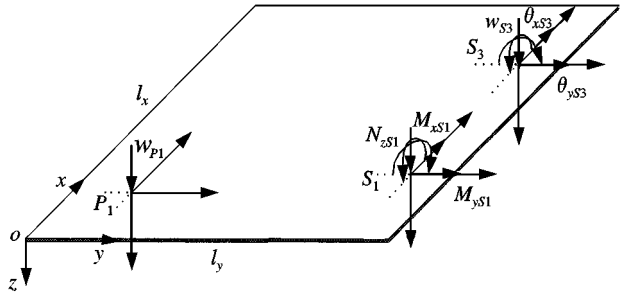

Figure A1. Notation of the displacement w at positions P_1 and S_3, and of the rotations θ_x, and θ_y, at positions S_3 when a plate is excited in flexure by a point force N_z and point moments M_x, and M_y, at position S_1.

APPENDIX A: PLATES MOBILITY MATRICES

The mobility matrices used into equations (53), (54), (57) and (58) have been derived using modal formulae for the point and transfer mobility terms of a plate excited only in bending as from reference [31].

The sub-mobility matrix between two generic positions, for example between positions S_3 and S_1 (see Figure A1) of the source plate is defined as follows:

$$\mathbf{M}_{S3S1}(\omega) = \begin{bmatrix} M_{wNz}^{S3S1}(\omega) & M_{wMx}^{S3S1}(\omega) & M_{wMy}^{S3S1}(\omega) \\ M_{\theta xNz}^{S3S1}(\omega) & M_{\theta xMx}^{S3S1}(\omega) & M_{\theta xMy}^{S3S1}(\omega) \\ M_{\theta yNz}^{S3S1}(\omega) & M_{\theta yMx}^{S3S1}(\omega) & M_{\theta yMy}^{S3S1}(\omega) \end{bmatrix}, \tag{A1}$$

where assuming the harmonic motion with time dependence of the form $\exp(j\omega t)$ and according to reference [31] the individual mobility terms are given by the following modal formulae:

$$M_{wNz}^{S3S1}(\omega) = \frac{\dot{\tilde{w}}_{S3}(\omega)}{\tilde{N}_{zS1}(\omega)} = j\omega \sum_{m=1}^{\infty} \sum_{n=1}^{\infty} \frac{\phi_{mn}(S_3)\phi_{mn}(S_1)}{\Lambda_{mn}[\omega_{fmn}^2(1+j\eta)-\omega^2]}, \tag{A2}$$

$$M_{wMx}^{S3S1}(\omega) = \frac{\dot{\tilde{w}}_{S3}(\omega)}{\tilde{M}_{xS1}(\omega)} = j\omega \sum_{m=1}^{\infty} \sum_{n=1}^{\infty} \frac{\phi_{mn}(S_3)\psi_{mn}^{(x)}(S_1)}{\Lambda_{mn}[\omega_{fmn}^2(1+j\eta)-\omega^2]}, \tag{A3}$$

$$M_{wMy}^{S3S1}(\omega) = \frac{\dot{\tilde{w}}_{S3}(\omega)}{\tilde{M}_{yS1}(\omega)} = j\omega \sum_{m=1}^{\infty} \sum_{n=1}^{\infty} \frac{\phi_{mn}(S_3)\psi_{mn}^{(y)}(S_1)}{\Lambda_{mn}[\omega_{fmn}^2(1+j\eta)-\omega^2]}, \tag{A4}$$

$$M_{\theta xNz}^{S3S1}(\omega) = \frac{\dot{\tilde{\theta}}_{xS3}(\omega)}{\tilde{N}_{zS1}(\omega)} = j\omega \sum_{m=1}^{\infty} \sum_{n=1}^{\infty} \frac{\psi_{mn}^{(x)}(S_3)\phi_{mn}(S_1)}{\Lambda_{mn}[\omega_{fmn}^2(1+j\eta)-\omega^2]}, \tag{A5}$$

$$M_{\theta yNz}^{S3S1}(\omega) = \frac{\dot{\tilde{\theta}}_{yS3}(\omega)}{\tilde{N}_{zS1}(\omega)} = j\omega \sum_{m=1}^{\infty} \sum_{n=1}^{\infty} \frac{\psi_{mn}^{(y)}(S_3)\phi_{mn}(S_1)}{\Lambda_{mn}[\omega_{fmn}^2(1+j\eta)-\omega^2]}, \tag{A6}$$

$$M_{\theta xMx}^{S3S1}(\omega) = \frac{\dot{\tilde{\theta}}_{xS3}(\omega)}{\tilde{M}_{xS1}(\omega)} = j\omega \sum_{m=1}^{\infty} \sum_{n=1}^{\infty} \frac{\psi_{mn}^{(x)}(S_3)\psi_{mn}^{(x)}(S_1)}{\Lambda_{mn}[\omega_{fmn}^2(1+j\eta)-\omega^2]}, \tag{A7}$$

$$M_{\theta xMy}^{S3S1}(\omega) = \frac{\tilde{\dot{\theta}}_{xS3}(\omega)}{\tilde{M}_{yS1}(\omega)} = \mathrm{j}\omega \sum_{m=1}^{\infty} \sum_{n=1}^{\infty} \frac{\psi_{mn}^{(x)}(S_3)\psi_{mn}^{(y)}(S_1)}{\Lambda_{mn}[\omega_{fmn}^2(1+\mathrm{j}\eta) - \omega^2]}, \tag{A8}$$

$$M_{\theta yMx}^{S3S1}(\omega) = \frac{\tilde{\dot{\theta}}_{yS3}(\omega)}{\tilde{M}_{xS1}(\omega)} = \mathrm{j}\omega \sum_{m=1}^{\infty} \sum_{n=1}^{\infty} \frac{\psi_{mn}^{(y)}(S_3)\psi_{m,n}^{(x)}(S_1)}{\Lambda_{mn}[\omega_{fmn}^2(1+\mathrm{j}\eta) - \omega^2]}, \tag{A9}$$

$$M_{\theta yMy}^{S3S1}(\omega) = \frac{\tilde{\dot{\theta}}_{yS3}(\omega)}{\tilde{M}_{yS1}(\omega)} = \mathrm{j}\omega \sum_{m=1}^{\infty} \sum_{n=1}^{\infty} \frac{\psi_{mn}^{(y)}(S_3)\psi_{m,n}^{(y)}(S_1)}{\Lambda_{mn}[\omega_{fmn}^2(1+\mathrm{j}\eta) - \omega^2]}, \tag{A10}$$

where ω is the circular frequency rad/s and η is the loss factor. The symbol " $\sim$ " indicates a complex value whose absolute value and phase denotes, respectively, the amplitude and phase of the harmonic variation in time at the driving frequency ω of the linear/angular velocity and force/moment excitation terms. A detailed description on how to calculate the natural frequencies ω_{fmn}, modal amplitudes ϕ_{mn}, modal slopes $\psi_{m,n}^{(x)}$, $\psi_{mn}^{(y)}$ and Λ_{mn} normalization factor for a freely supported thin plate can be found in section 3·7 of reference [31].

The mobility matrix of equations (57) and (58) relates only the out-of-plane velocity component $\dot{w}_j$ at the five monitoring positions of the source and receiver plates to the mounting junctions positions force and moment parameters, therefore the sub-mobility matrix between a monitoring position and a mounting junction position, for example between positions P_1 and S_1 of the source plate, is defined as follows:

$$\mathbf{M}_{P1S1}(\omega) = \lfloor M_{wNz}^{P1S1}(\omega) \quad M_{wMx}^{P1S1}(\omega) \quad M_{wMy}^{P1S1}(\omega) \rfloor. \tag{A11}$$

APPENDIX B: MOUNTING SYSTEM IMPEDANCE AND EXCITATION MATRICES

The impedance matrix used into equations (55) and (56) has been derived by modelling each mount as a distributed one-dimensional element on which longitudinal and bending waves propagate. The impedance terms have been calculated by deriving the exact solution in closed form of the standard second order wave equation of longitudinal waves and of the Euler–Bernoulli fourth order wave equation of flexural waves [32], assuming the beam element either with both ends freely suspended or both ends pinned in x and y directions.

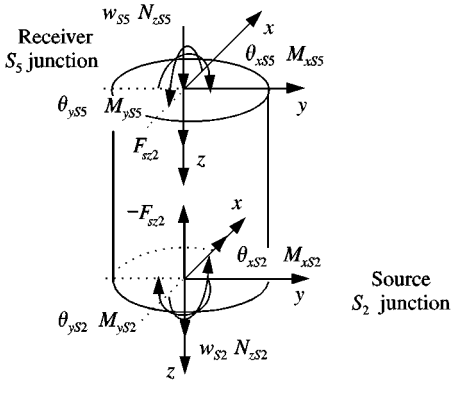

Figure A2. Notation of the displacement w and rotations θ_x, and θ_y, point force N_z and point moments M_x, and M_y at the top and bottom junctions of mount number 2 of the system shown in Figure 2.

As discussed in section 3, it has been chosen to neglect 3 d.o.f.s at each mount junction. The following kinematic and dynamic parameters are not taken into account in the matrix formulation: first, the angular velocity and moment in z direction, $\dot{\theta}_z$ and M_z; second, the linear velocity and force in x direction, $\dot{u}$ and N_x, and third, the linear velocity and force in y direction, $\dot{v}$ and N_y. Therefore, at each end of the mounts only the linear velocity $\dot{w}$ and angular velocities, $\dot{\theta}_x$ and $\dot{\theta}_y$, and only the point force N_z and point moments, M_x and M_y, are accounted for. Figure A2 shows the notation of these three kinematic and dynamic parameters at the top and bottom junctions of the mount number 2 whose junctions are denoted by the symbols S_2 (bottom junction) and S_5 (top junction).

If all six kinematic and dynamic parameters are accounted for at each end of a freely suspended mount element, the 12×12 impedance matrix would be defined as in the following relation:

$$\begin{bmatrix} N_{xS2} \\ N_{yS2} \\ N_{zS2} \\ M_{xS2} \\ M_{yS2} \\ M_{zS2} \\ N_{xS5} \\ N_{yS5} \\ N_{zS5} \\ M_{xS5} \\ M_{yS5} \\ M_{zS5} \end{bmatrix} = \begin{bmatrix} Z_{Nxu}^{S2S2} & 0 & 0 & 0 & Z_{Nx\theta y}^{S2S2} & 0 & Z_{Nxu}^{S2S5} & 0 & 0 & 0 & Z_{Nx\theta y}^{S2S5} & 0 \\ 0 & Z_{Nyv}^{S2S2} & 0 & Z_{Ny\theta x}^{S2S2} & 0 & 0 & 0 & Z_{Nyv}^{S2S5} & 0 & Z_{Ny\theta x}^{S2S5} & 0 & 0 \\ 0 & 0 & Z_{Nzw}^{S2S2} & 0 & 0 & 0 & 0 & 0 & Z_{Nzw}^{S2S5} & 0 & 0 & 0 \\ 0 & Z_{Mxv}^{S2S2} & 0 & Z_{Mx\theta x}^{S2S2} & 0 & 0 & 0 & Z_{Mxv}^{S2S5} & 0 & Z_{Mx\theta x}^{S2S5} & 0 & 0 \\ Z_{Myu}^{S2S2} & 0 & 0 & 0 & Z_{My\theta y}^{S2S2} & 0 & Z_{Myu}^{S2S5} & 0 & 0 & 0 & Z_{My\theta y}^{S2S5} & 0 \\ 0 & 0 & 0 & 0 & 0 & Z_{Mz\theta z}^{S2S2} & 0 & 0 & 0 & 0 & 0 & Z_{Mz\theta z}^{S2S5} \\ Z_{Nxu}^{S5S2} & 0 & 0 & 0 & Z_{Nx\theta y}^{S5S2} & 0 & Z_{Nxu}^{S5S5} & 0 & 0 & 0 & Z_{Nx\theta y}^{S5S5} & 0 \\ 0 & Z_{Nyv}^{S5S2} & 0 & Z_{Ny\theta x}^{S5S2} & 0 & 0 & 0 & Z_{Nyv}^{S5S5} & 0 & Z_{Ny\theta x}^{S5S5} & 0 & 0 \\ 0 & 0 & Z_{Nzw}^{S5S2} & 0 & 0 & 0 & 0 & 0 & Z_{Nzw}^{S5S5} & 0 & 0 & 0 \\ 0 & Z_{Mxv}^{S5S2} & 0 & Z_{Mx\theta x}^{S5S2} & 0 & 0 & 0 & Z_{Mxv}^{S5S5} & 0 & Z_{Mx\theta x}^{S5S5} & 0 & 0 \\ Z_{Myu}^{S5S2} & 0 & 0 & 0 & Z_{My\theta y}^{S5S2} & 0 & Z_{Myu}^{S5S5} & 0 & 0 & 0 & Z_{My\theta y}^{S5S5} & 0 \\ 0 & 0 & 0 & 0 & 0 & Z_{Mz\theta z}^{S5S2} & 0 & 0 & 0 & 0 & 0 & Z_{Mz\theta z}^{S5S5} \end{bmatrix} \begin{bmatrix} \dot{u}_{S2} \\ \dot{v}_{S2} \\ \dot{w}_{S2} \\ \dot{\theta}_{xS2} \\ \dot{\theta}_{yS2} \\ \dot{\theta}_{zS2} \\ \dot{u}_{S5} \\ \dot{v}_{S5} \\ \dot{w}_{S5} \\ \dot{\theta}_{xS5} \\ \dot{\theta}_{yS5} \\ \dot{\theta}_{zS5} \end{bmatrix}, \tag{B1}$$

where the six kinematic (linear and angular velocities) and dynamic (force and moment excitations) parameters at each end of the mount are oriented as in the Figure A3.

The four impedance matrices $\mathbf{Z}_{11}$, $\mathbf{Z}_{12}$, $\mathbf{Z}_{21}$ and $\mathbf{Z}_{22}$ to be used into equations (55) and (56) can be obtained from the impedance matrix of equation (B1) by removing the rows and columns for the d.o.f.s neglected. Therefore,

$$\mathbf{Z}_{11} = \begin{bmatrix} \bar{Z}_{Nzw}^{S2S2} & 0 & 0 \\ 0 & \bar{Z}_{Mx\theta x}^{S2S2} & 0 \\ 0 & 0 & \bar{Z}_{My\theta y}^{S2S2} \end{bmatrix}, \qquad \mathbf{Z}_{12} = \begin{bmatrix} \bar{Z}_{Nzw}^{S2S5} & 0 & 0 \\ 0 & \bar{Z}_{Mx\theta x}^{S2S5} & 0 \\ 0 & 0 & \bar{Z}_{My\theta y}^{S2S5} \end{bmatrix}, \tag{B2, B3}$$

$$\mathbf{Z}_{21} = \begin{bmatrix} \bar{Z}_{Nzw}^{S5S2} & 0 & 0 \\ 0 & \bar{Z}_{Mx\theta x}^{S5S2} & 0 \\ 0 & 0 & \bar{Z}_{My\theta y}^{S5S2} \end{bmatrix}, \qquad \mathbf{Z}_{22} = \begin{bmatrix} \bar{Z}_{Nzw}^{S5S5} & 0 & 0 \\ 0 & \bar{Z}_{Mx\theta x}^{S5S5} & 0 \\ 0 & 0 & \bar{Z}_{My\theta y}^{S5S5} \end{bmatrix}, \tag{B4, B5}$$

However, some care has to be taken while doing this operation. The impedance terms related to the axial velocity $\dot{w}_{Sj}$ and force N_{zSi} parameters remains the same as those of the 12×12 impedance matrix (e.g., $\bar{Z}_{Nzw}^{SiSj} = Z_{Nzw}^{SiSj}$). These four point and transfer impedances, related to longitudinal waves, are given by the following relations:

$$Z_{Nzw}^{S2S2}(\omega) = \frac{\tilde{N}_{zS2}(\omega)}{\tilde{\dot{w}}_{S2}(\omega)} = Z_{Nzw}^{S5S5}(\omega) = \frac{\tilde{N}_{zS5}(\omega)}{\tilde{\dot{w}}_{S5}(\omega)} = \frac{1}{\mathrm{j}\omega} \frac{E_m A_m k_{lm} \lambda_1}{\lambda_2} \tag{B6}$$

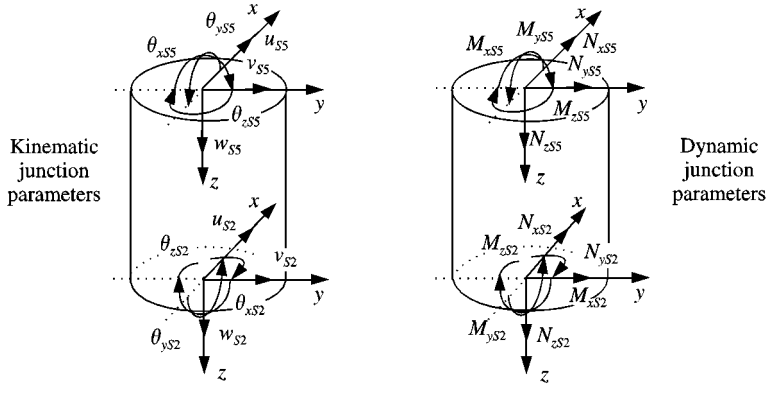

Figure A3 Notation of the six kinematic (linear and angular displacements) and dynamic (force and moment excitations) parameters at each end of mount number 2 of the system shown in Figure 2.

$$Z_{Nzw}^{S2S5}(\omega) = \frac{\tilde{N}_{zS5}(\omega)}{\dot{\tilde{w}}_{S2}(\omega)} = Z_{Nzw}^{S5S2}(\omega) = \frac{\tilde{N}_{zS2}(\omega)}{\dot{\tilde{w}}_{S5}(\omega)} = -\frac{1}{\mathrm{j}\omega}\frac{E_m A_m k_{lm}}{\lambda_2} \tag{B7}$$

where E_m is the Young's modulus of elasticity, A_m is the mount cross-sectional area and ω is the circular frequency (rad/s). $k_{lm} = \omega/c_{lm} = \omega/\sqrt{E_m/\rho_m}$ is the longitudinal wave number, c_{lm} is the phase velocity of longitudinal waves and ρ_m is the density of the material. The two parameters λ_1 and λ_2 are given by

$$\lambda_1 = \cos k_{lm} h_m, \qquad \lambda_2 = \sin k_{lm} h_m \tag{B8, B9}$$

where h_m is the mount height.

Neglecting the angular velocity and moment in the z direction at the two ends of the mount element, $\dot{\theta}_z$ and M_z, respectively, implies that the two driving point and two transfer impedance terms related to torsional vibration are not accounted for in the impedance matrix of the mount element. Therefore, the terms $Z_{Mz\theta z}^{SiSj}$ are set to zero and the rows and columns number 6 and 12 of the impedance matrix given in equation (B1) are taken out.

Neglecting the velocities in x and y directions, $\dot{u}$ and $\dot{v}$, and the force components N_x and N_y cannot be treated so simply. In fact, in order to derive the four impedance matrices $\mathbf{Z}_{11}$, $\mathbf{Z}_{12}$, $\mathbf{Z}_{21}$ and $\mathbf{Z}_{22}$, it is not sufficient to take off the impedance terms related to those kinematic and dynamic parameters (e.g., set $Z_{Nxu}^{SiSj} = Z_{Nyv}^{SiSj} = Z_{Nx\theta y}^{SiSj} = Z_{Nyv}^{SiSj} = Z_{Mxv}^{SiSj} = Z_{Myu}^{SiSj} = 0$ and delete row and column numbers 1, 2, 7 and 8 of the impedance matrix given in equation (B1)).

This point is discussed by O'Hara [33] and Rubin [12], who discuss why it is not generally correct to pick out only some of the elements of a $n \times n$ impedance matrix, which relates force and velocity parameters that are coupled, in order to build up a smaller $m \times m$ impedance matrix. This is because the elements of the $n \times n$ or $m \times m$ impedance matrices are derived by imposing a "constraint" on the linear or angular velocity parameters accounted for in the matrix relation $\mathbf{f} = \mathbf{Z}\mathbf{v}$. For example, the impedance term $Z_{\theta xMx}^{S5S2}$ for the 6×6 impedance matrix is calculated assuming the following constraints:

$$Z_{Mx\theta x}^{S2S5} = \frac{\tilde{M}_{xS2}}{\tilde{\theta}_{xS5}} \quad \text{and} \quad w_{S2} = w_{S5} = \theta_{xS2} = \theta_{yS2} = \theta_{yS5} = 0 \tag{B10}$$

(note that no constraint is placed on u_{S2}, u_{S5}, v_{S2}, v_{S5}, θ_{zS2}, θ_{zS5} which can take any value) and for the 12×12 impedance matrix,

$$Z^{S2S5}_{Mx\theta x} = \frac{\tilde{M}_{xS2}}{\tilde{\theta}_{xS5}} \quad \text{and} \quad u_{S2} = u_{S5} = v_{S2} = v_{S5} = w_{S2} = w_{S5}$$

$$= \theta_{xS2} = \theta_{yS2} = \theta_{yS5} = \theta_{zS2} = \theta_{zS5} = 0. \tag{B11}$$

Thus, the $Z^{S2S5}_{Mx\theta x}$ term differs when calculated with either equation (B10) or equation (B11). This is because the one dimensional mounting element is constrained in a different way in the two cases.

If instead, a mobility relation $\mathbf{v} = \mathbf{Mf}$ is considered, it can be shown that the reduction from a m to a $n < m$ d.o.f.s mobility matrix relation can be carried out simply by "collapsing" the mobility matrix $\mathbf{M}_{m \times m}$ into the $\mathbf{M}_{n \times n}$. In fact, if the mobility term $M^{S2S5}_{\theta xMx}$ is considered, it can be noticed that whether this term is calculated for a 6×6 or a 12×12 mobility matrix (e.g., either only 3 or all 6 d.o.f.s are accounted for in the matrix relation) the same result is obtained since only the excitations are constrained in a different way. So for the 6×6 mobility matrix

$$M^{S2S5}_{\theta xMx} = \frac{\tilde{\dot{\theta}}_{xS5}}{\tilde{M}_{xS2}} \quad \text{and} \quad N_{zS2} = N_{zS5} = M_{xS2} = M_{ySS2} = M_{yS5} = 0 \tag{B12}$$

(note that no constraint is placed on the excitation parameters N_{xS2}, N_{xS5}, N_{yS2}, N_{yS5}, M_{zS2}, M_{zS5}, although they could be implicitly assumed to be zero) and for the 12×12 mobility matrix

$$M^{S2S5}_{\theta xMx} = \frac{\tilde{\dot{\theta}}_{xS5}}{\tilde{M}_{xS2}} \quad \text{and} \quad N_{xS2} = N_{xS5} = N_{yS2} = N_{yS5} = N_{zS2} = N_{zS5} = M_{xS2} = M_{yS2}$$

$$= M_{yS5} = M_{zS2} = M_{zS5} = 0. \tag{B13}$$

Therefore, the 6×6 mobility matrix $\mathbf{M}_{6 \times 6}$ is correct even if its elements are picked up from the 12×12 mobility matrix $\mathbf{M}_{12 \times 12}$.

In conclusion, the reduction of a $m \times m$ impedance matrix to a smaller $n \times n$ matrix is possible only if the kinematic and dynamic parameters of the impedance relation $\mathbf{f} = \mathbf{Zv}$ are uncoupled. This is not the case for mobility matrices. It is in fact possible to reduce a $m \times m$ mobility matrix to a smaller $n \times n$ matrix without the need of recalculating the mobility terms even if the kinematic and dynamic parameters of the mobility relation $\mathbf{v} = \mathbf{Zf}$ are coupled. Therefore, for the specific case examined in this appendix, the impedance terms $\bar{Z}^{SjSi}_{Mx\theta x}$, $\bar{Z}^{SjSi}_{My\theta y}$ cannot be derived directly from the equivalent ones of the 12×12 impedance matrix of equation (B1). For their exact calculation there are two options: either they are analytically calculated assuming the pertinent boundary conditions at each end of the mount element (e.g., by constraining the $\dot{u}$ and $\dot{v}$ linear velocities and the N_x, and N_y force components) or they are calculated by inverting a reduced mobility matrix $\mathbf{M}_{6 \times 6}$ which has been directly derived from the complete mobility matrix $\mathbf{M}_{12 \times 12}$ which refers to all six kinematic and dynamic parameters at each end of the mount element.

However, there is a second problem that has to be considered before moving on to calculate the impedance terms $\bar{Z}^{SjSi}_{Mx\theta x}$ and $\bar{Z}^{SjSi}_{My\theta y}$. Flexural waves in a beam, unlike the other wave types, are represented by four field parameters instead of two [32]. For example the flexural vibration in the x–z plane is represented by the linear velocity and force in x direction, $\dot{u}$ and N_x, and the angular velocity and moment in y direction, $\dot{\theta}_y$ and M_y. These four variables are coupled so that the angular velocity $\dot{\theta}_y$ at one end of the mount element, let

us say junction S_2, due to a collocated moment M_y can be found only if the linear velocity $\dot{u}$ and force N_x at the two ends are fixed and if the angular velocity and moment in y direction, $\dot{\theta}_y$ and M_y, at the opposite end of the one where the angular velocity is determined, junction S_5, are specified. Therefore, even when the mobility matrix for the reduced case accounting for 3 d.o.f.s at each end of the mount is calculated, in order to derive the mobility term $\bar{M}^{S2S2}_{\theta yMy} = \dot{\theta}_{yS2}/M_{ySj}|_{M_{ys5}=0}$, the values of the linear velocity $\dot{u}$ and force N_x at the two ends has to be specified. The boundary conditions for the angular velocity $\dot{\theta}_y$ and moment M_y at the junction S_5 are set to be as those of a freely suspended beam so that $\dot{\theta}_{yS5} \neq 0$ and $M_{ySj} = 0$. The other four boundary conditions requires some thought before they are fixed. They are in fact neglected in the formulation of the problem (see section 4). The problem is to transform the verb "to neglect" into a mathematical expression. Indeed, there are four possible choices for the linear velocity $\dot{u}$ and force N_x at the two ends of the mount element: first $\dot{u}_{Sj} = 0$ and $N_{xSj} = 0$; second, $\dot{u}_{Sj} \neq 0$ and $N_{xSj} \neq 0$; third, $\dot{u}_{Sj} = 0$ and $N_{xSj} \neq 0$ and fourth $\dot{u}_{Sj} \neq 0$ and $N_{xSj} = 0$. The first two cannot be imposed since the solution of the wave equation would be undetermined. The third and the fourth one are instead compatible with the flexural wave equation and, when associated to the boundary condition chosen for the angular velocity and moment at the two ends, they give rise to the study of either a freely suspended beam whose boundary conditions at the two ends are $\dot{\theta}_{yS5} \neq 0$, $M_{yS5} = 0$, $\dot{u}_{S2} \neq 0$ and $N_{xS2} = 0$ or the study of a pinned–pinned beam having instead the following boundary conditions at the two ends $\dot{\theta}_{yS5} \neq 0$, $M_{ySj} = 0$, $\dot{u}_{Sj} = 0$ and $N_{xSj} \neq 0$.

In view of the above-mentioned problem about the reduction of the number of rows and columns of an impedance matrix, the impedance terms $\bar{Z}^{SjSi}_{Mx\theta x}$, $\bar{Z}^{SjSi}_{My\theta y}$ have been derived by inverting the mobility matrix given in the following expression:

$$\begin{Bmatrix} \dot{w}_{S2} \\ \dot{\theta}_{xS2} \\ \dot{\theta}_{yS2} \\ \dot{w}_{S5} \\ \dot{\theta}_{xS5} \\ \dot{\theta}_{yS5} \end{Bmatrix} = \begin{bmatrix} M^{S2S2}_{wNz} & 0 & 0 & M^{S2S5}_{wNz} & 0 & 0 \\ 0 & M^{S2S2}_{\theta xMx} & 0 & 0 & M^{S2S5}_{\theta xMx} & 0 \\ 0 & 0 & M^{S2S2}_{\theta yMy} & 0 & 0 & M^{S2S5}_{\theta yMy} \\ M^{S5S2}_{wNz} & 0 & 0 & M^{S5S5}_{wNz} & 0 & 0 \\ 0 & M^{S5S2}_{\theta xMx} & 0 & 0 & M^{S5S5}_{\theta xMx} & 0 \\ 0 & 0 & M^{S5S2}_{\theta yMy} & 0 & 0 & M^{S5S5}_{\theta yMy} \end{bmatrix} \begin{Bmatrix} N_{zS2} \\ M_{xS2} \\ M_{yS2} \\ N_{zS5} \\ M_{xS5} \\ M_{yS5} \end{Bmatrix}. \tag{B14}$$

This 6×6 mobility matrix has been derived exactly by cancelling row and column numbers 1, 2, 6–8 and 12 of the complete 12×12 mobility matrix assuming that the mount element freely suspended:

$$\begin{bmatrix} \dot{u}_{S2} \\ \dot{v}_{S2} \\ \dot{w}_{S2} \\ \dot{\theta}_{xS2} \\ \dot{\theta}_{yS2} \\ \dot{\theta}_{zS2} \\ \dot{u}_{S5} \\ \dot{v}_{S5} \\ \dot{w}_{S5} \\ \dot{\theta}_{xS5} \\ \dot{\theta}_{yS5} \\ \dot{\theta}_{zS5} \end{bmatrix} = \begin{bmatrix} M^{S2S2}_{uNx} & 0 & 0 & 0 & M^{S2S2}_{uMy} & 0 & M^{S2S5}_{uNx} & 0 & 0 & 0 & M^{S2S5}_{uMy} & 0 \\ 0 & M^{S2S2}_{vNy} & 0 & M^{S2S2}_{vMx} & 0 & 0 & 0 & M^{S2S5}_{vNy} & 0 & M^{S2S5}_{vMx} & 0 & 0 \\ 0 & 0 & M^{S2S2}_{wNz} & 0 & 0 & 0 & 0 & 0 & M^{S2S5}_{wNz} & 0 & 0 & 0 \\ 0 & M^{S2S2}_{\theta xNy} & 0 & M^{S2S2}_{\theta xMx} & 0 & 0 & 0 & M^{S2S5}_{\theta xNy} & 0 & M^{S2S5}_{\theta xMx} & 0 & 0 \\ M^{S2S2}_{\theta yNx} & 0 & 0 & 0 & M^{S2S2}_{\theta yMy} & 0 & M^{S2S5}_{\theta yNx} & 0 & 0 & 0 & M^{S2S5}_{\theta yMy} & 0 \\ 0 & 0 & 0 & 0 & 0 & M^{S2S2}_{\theta zMz} & 0 & 0 & 0 & 0 & 0 & M^{S2S5}_{\theta zMz} \\ M^{S5S2}_{uNx} & 0 & 0 & 0 & M^{S5S2}_{uMy} & 0 & M^{S5S5}_{uNx} & 0 & 0 & 0 & M^{S5S5}_{uMy} & 0 \\ 0 & M^{S5S2}_{vNy} & 0 & M^{S5S2}_{vMx} & 0 & 0 & 0 & M^{S5S5}_{vNy} & 0 & M^{S5S5}_{vMx} & 0 & 0 \\ 0 & 0 & M^{S5S2}_{wNz} & 0 & 0 & 0 & 0 & 0 & M^{S5S5}_{wNz} & 0 & 0 & 0 \\ 0 & M^{S5S2}_{\theta xNy} & 0 & M^{S5S2}_{\theta xMx} & 0 & 0 & 0 & M^{S5S5}_{\theta xNy} & 0 & M^{S5S5}_{\theta xMx} & 0 & 0 \\ M^{S5S2}_{\theta yNx} & 0 & 0 & 0 & M^{S5S2}_{\theta yMy} & 0 & M^{S5S5}_{\theta yNx} & 0 & 0 & 0 & M^{S5S5}_{\theta yMy} & 0 \\ 0 & 0 & 0 & 0 & 0 & M^{S5S2}_{\theta zMz} & 0 & 0 & 0 & 0 & 0 & M^{S5S5}_{\theta zMz} \end{bmatrix} \begin{bmatrix} N_{xS2} \\ N_{yS2} \\ N_{zS2} \\ M_{xS2} \\ M_{yS2} \\ M_{zS2} \\ N_{xS5} \\ N_{yS5} \\ N_{zS5} \\ M_{xS5} \\ M_{yS5} \\ M_{zS5} \end{bmatrix}, \tag{B15}$$

All the mobility terms of this mobility matrix can be found in Table 7.1(c) of Bishop and Johnson [34].

With reference to the other problem discussed above, it has been decided to also calculate the impedance terms $\bar{Z}^{SjSi}_{Mx\theta x}$, $\bar{Z}^{SjSi}_{My\theta y}$ for a beam element with both ends pinned in x and y directions. The same procedure has been followed as for the case of a freely suspended element. First, the reduced 6×6 mobility matrix has been derived for a mount element with each end pinned in x and y directions and second, this mobility matrix has been inverted in order to give the equivalent impedance matrix with the exact $\bar{Z}^{SjSi}_{Mx\theta x}$, $\bar{Z}^{SjSi}_{My\theta y}$ impedance terms.

With reference to the freely suspended boundary condition (e.g., $\dot{u}_{Sj} \neq 0$, $\dot{v}_{Sj} \neq 0$, $\dot{\theta}_{xSj} \neq 0$, $\dot{\theta}_{ySj} \neq 0$ and $N_{xSj} = 0$, $N_{ySj} = 0$, $M_{xSj} = 0$, $M_{ySj} = 0$) the eight impedance elements have been calculated as follows:

$$Z^{S2S2}_{Mx\theta x}(\omega) = \frac{\tilde{M}_{xS2}(\omega)}{\tilde{\dot{\theta}}_{xS2}(\omega)} = Z^{S5S5}_{Mx\theta x}(\omega) = \frac{\tilde{M}_{xS5}(\omega)}{\tilde{\dot{\theta}}_{xS5}(\omega)} = \frac{1}{\mathrm{j}\omega} \frac{E_m I_m k_{fm} \varphi_3 \varphi_6}{\varphi_6^2 - \varphi_7^2}, \tag{B16}$$

$$Z^{S2S2}_{My\theta y}(\omega) = \frac{\tilde{M}_{yS2}(\omega)}{\tilde{\dot{\theta}}_{yS2}(\omega)} = Z^{S5S5}_{My\theta y}(\omega) = \frac{\tilde{M}_{yS5}(\omega)}{\tilde{\dot{\theta}}_{yS5}(\omega)} = -\frac{1}{\mathrm{j}\omega} \frac{E_m I_m k_{fm} \varphi_3 \varphi_7}{\varphi_6^2 - \varphi_7^2}, \tag{B17}$$

$$Z^{S2S5}_{Mx\theta x}(\omega) = \frac{\tilde{M}_{xS2}(\omega)}{\tilde{\dot{\theta}}_{xS5}(\omega)} = Z^{S5S2}_{Mx\theta x}(\omega) = \frac{\tilde{M}_{xS5}(\omega)}{\tilde{\dot{\theta}}_{xS2}(\omega)} = -\frac{1}{\mathrm{j}\omega} \frac{E_m I_m k_{fm} \varphi_3 \varphi_7}{\varphi_6^2 - \varphi_7^2}, \tag{B18}$$

$$Z^{S2S5}_{My\theta y}(\omega) = \frac{\tilde{M}_{yS2}(\omega)}{\tilde{\dot{\theta}}_{yS5}(\omega)} = Z^{S5S2}_{My\theta y}(\omega) = \frac{\tilde{M}_{yS5}(\omega)}{\tilde{\dot{\theta}}_{yS2}(\omega)} = \frac{1}{\mathrm{j}\omega} \frac{E_m I_m k_{fm} \varphi_3 \varphi_6}{\varphi_6^2 - \varphi_7^2}. \tag{B19}$$

where

$$\varphi_3 = \cos k_{fm} h_m \cosh k_{fm} h_m - 1, \tag{B20}$$

$$\varphi_6 = \cos k_{fm} h_m \sinh k_{fm} h_m + \sin k_{fm} h_m \cosh k_{fm} h_m \tag{B21}$$

$$\varphi_7 = \sin k_{fm} h_m + \sinh k_{fm} h_m \tag{B22}$$

and $k_{fm} = \omega / c_{fm} = \sqrt[4]{\omega^2 m'/B}$ is the flexural wave number, $c_{fm} = \sqrt[2]{\omega}\sqrt[4]{B/m'}$ is the phase velocity of flexural waves, $B = E_m I_m$ is the bending stiffness of the mount, $I_m = I_x = I_y = \pi a_m^4/4$ is the area moment of inertia of the circular mount cross-section with radius a, and $m' = \rho_m A_m$ is the density per unit area of the material.

With reference to the boundary condition (e.g., $\dot{u}_{Sj} = 0$, $\dot{v}_{Sj} = 0$, $\dot{\theta}_{xSj} \neq 0$, $\dot{\theta}_{ySj} \neq 0$, and $N_{xSj} = 0$, $N_{ySj} = 0$, $M_{xSy} = 0$, $M_{ySy} = 0$) pinned in x and y directions, the eight impedance elements have been calculated as follows:

$$Z^{S2S2}_{Mx\theta x}(\omega) = \frac{\tilde{M}_{xS2}(\omega)}{\tilde{\dot{\theta}}_{xS2}(\omega)} = Z^{S5S5}_{Mx\theta x}(\omega) = \frac{\tilde{M}_{xS5}(\omega)}{\tilde{\dot{\theta}}_{xS5}(\omega)} = \frac{2}{\mathrm{j}\omega} \frac{E_m I_m k_{fm} \varphi_1 \varphi_5}{\varphi_5^2 - \varphi_8^2}, \tag{B23}$$

$$Z^{S2S2}_{My\theta y}(\omega) = \frac{\tilde{M}_{yS2}(\omega)}{\tilde{\dot{\theta}}_{yS2}(\omega)} = Z^{S5S5}_{My\theta y}(\omega) = \frac{\tilde{M}_{yS5}(\omega)}{\tilde{\dot{\theta}}_{yS5}(\omega)} = -\frac{2}{\mathrm{j}\omega} \frac{E_m I_m k_{fm} \varphi_1 \varphi_8}{\varphi_5^2 - \varphi_8^2}, \tag{B24}$$

$$Z^{S2S5}_{Mx\theta x}(\omega) = \frac{\tilde{M}_{xS2}(\omega)}{\tilde{\dot{\theta}}_{xS5}(\omega)} = Z^{S5S2}_{Mx\theta x}(\omega) = \frac{\tilde{M}_{xS5}(\omega)}{\tilde{\dot{\theta}}_{xS2}(\omega)} = -\frac{2}{\mathrm{j}\omega} \frac{E_m I_m k_{fm} \varphi_1 \varphi_8}{\varphi_5^2 - \varphi_8^2}, \tag{B25}$$

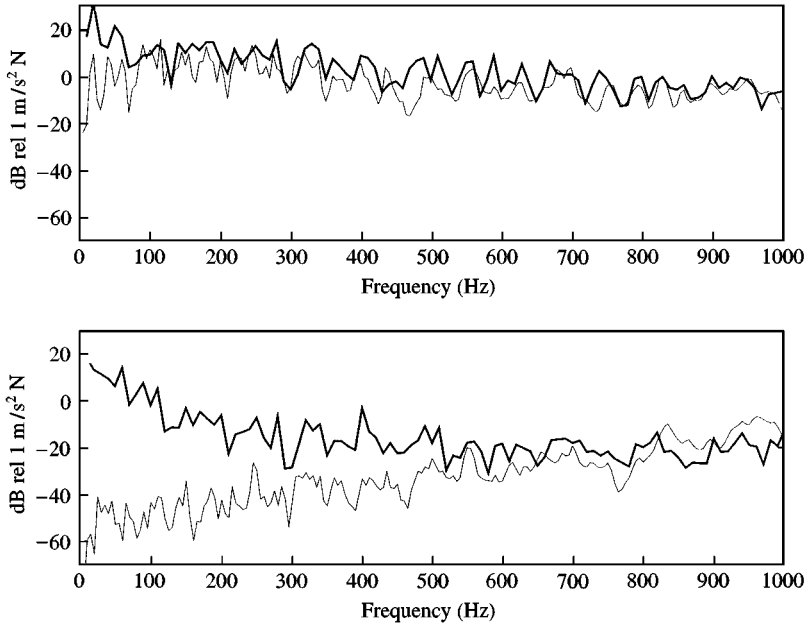

Figure A4. Estimate of the receiver K_{Er} kinetic energy without (top plot) and with (bottom plot) active control of the out-of-plane velocities at the receiver mounts junction when the primary force F_{p3} is exciting the two-panel system with three-rubber mounts having block masses at the ends: ———, experimental predictions, ——, simulations assuming the mount element freely suspended.

$$Z^{S2S5}_{My\theta y}(\omega) = \frac{\tilde{M}_{yS2}(\omega)}{\tilde{\dot{\theta}}_{yS5}(\omega)} = Z^{S5S2}_{My\theta y}(\omega) = \frac{\tilde{M}_{yS5}(\omega)}{\tilde{\dot{\theta}}_{yS2}(\omega)} = \frac{2}{\mathrm{j}\omega}\frac{E_m I_m k_{fm}\varphi_1\varphi_5}{\varphi_5^2 - \varphi_8^2}. \tag{B26}$$

where

$$\varphi_1 = \sin k_{fm}h_m \sinh k_{fm}h_m \tag{B27}$$

$$\varphi_5 = \cos k_{fm}h_m \sinh k_{fm}h_m - \sin k_{fm}h_m \cosh k_{fm}h_m \tag{B28}$$

$$\varphi_8 = \sin k_{fm}h_m - \sinh k_{fm}h_m. \tag{B29}$$

Therefore, two set of impedance terms $\bar{Z}^{SjSi}_{Mx\theta x}$ and $\bar{Z}^{SjSi}_{My\theta y}$ have been calculated for the impedance matrices $\mathbf{Z}_{11}$, $\mathbf{Z}_{12}$, $\mathbf{Z}_{21}$ and $\mathbf{Z}_{22}$ to be used into equations (55) and (56).

The results obtained with the two sets of impedance matrices have been compared with measured data (as in section 5) in order to estimate which one between the freely suspended and the pinned in x and y directions boundary conditions is the most representative one for the system studied in this paper.

The comparison has been carried out for the two-plate system shown in Figure 2 having either a rubber or aluminium mount with lumped masses at the top and bottom ends ($W_t = 9{\cdot}8 \times 10^{-3}$ kg, $W_b = 3{\cdot}1 \times 10^{-3}$ kg) and with inertial control actuators acting at the top end of the mounts. The control strategy considered is the cancellation of axial velocities at the top of the mounts. The primary excitation has been chosen at position P_3. Figures A4

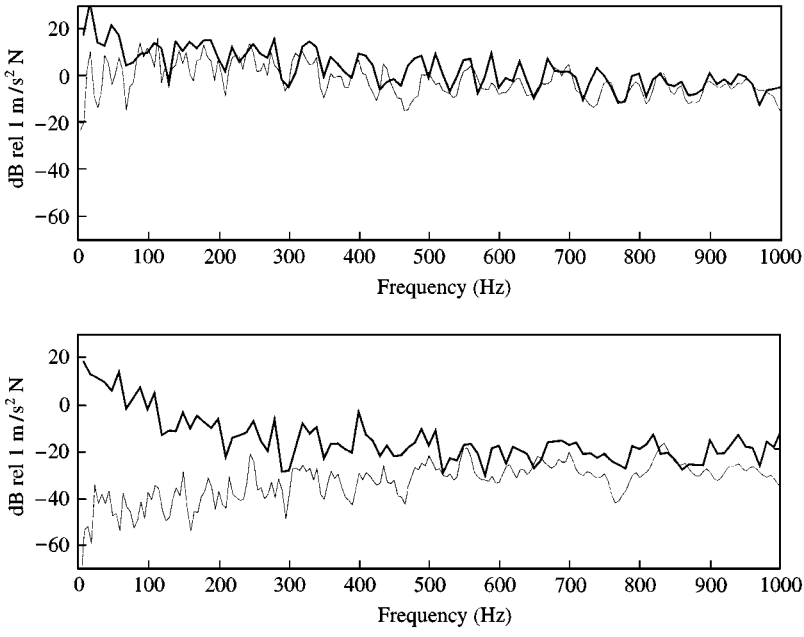

Figure A5. Estimate of the receiver K_{Er} kinetic energy without (top plot) and with (bottom plot) active control of the out-of-plane velocities at the receiver mounts junction when the primary force F_{p3} is exciting the two-panel system with three-rubber mounts having block masses at the ends: ———, experimental predictions, ——, simulations assuming the mount element pinned in x and y directions.

and A5 shows the estimate of the receiver K_{Er} kinetic energy without (top plot) and with (bottom plot) active control for the isolator systems with rubber mounts when the four impedance matrices $\mathbf{Z}_{11}$, $\mathbf{Z}_{12}$, $\mathbf{Z}_{21}$ and $\mathbf{Z}_{22}$ have been calculated for a freely suspended or pinned mount element. Figures A6 and A7 shows the same type of plots but for the case where the four impedance matrices $\mathbf{Z}_{11}$, $\mathbf{Z}_{12}$, $\mathbf{Z}_{21}$ and $\mathbf{Z}_{22}$ have been calculated for an aluminium mount element.

From these plots it can be seen that when there are no control forces the results obtained with either types of impedance matrix are very good. When the control forces are active, the result which line up best with the experimental data are achieved when the four impedance matrices $\mathbf{Z}_{11}$, $\mathbf{Z}_{12}$, $\mathbf{Z}_{21}$ and $\mathbf{Z}_{22}$ are calculated for a freely suspended mount. When there is no control, the main contribution to the vibration transmission is given by the axial vibration of the mount. Thus, the modelling of the impedance parameters related to the angular d.o.f.s is not crucial. When control is applied, however, the axial vibration of the mount at the junction with the receiver plate is cancelled, so that the vibration transmission is controlled by the angular displacements. In this case, the modelling of the impedance parameters related to the angular d.o.f.s is important since it determines the level of vibration transmission after control.

In view of these results, it has been chosen to present in this paper the results obtained by using the matrix model with the four impedance matrices $\mathbf{Z}_{11}$, $\mathbf{Z}_{12}$, $\mathbf{Z}_{21}$ and $\mathbf{Z}_{22}$ calculated for a freely suspended mount.

If the inertial effects due to the components used to connect the mounting system to the plates and to connect force and velocity sensors at the top of the mounts are also accounted and modelled as a pair of rectangular parallelepiped block masses connected at the mount

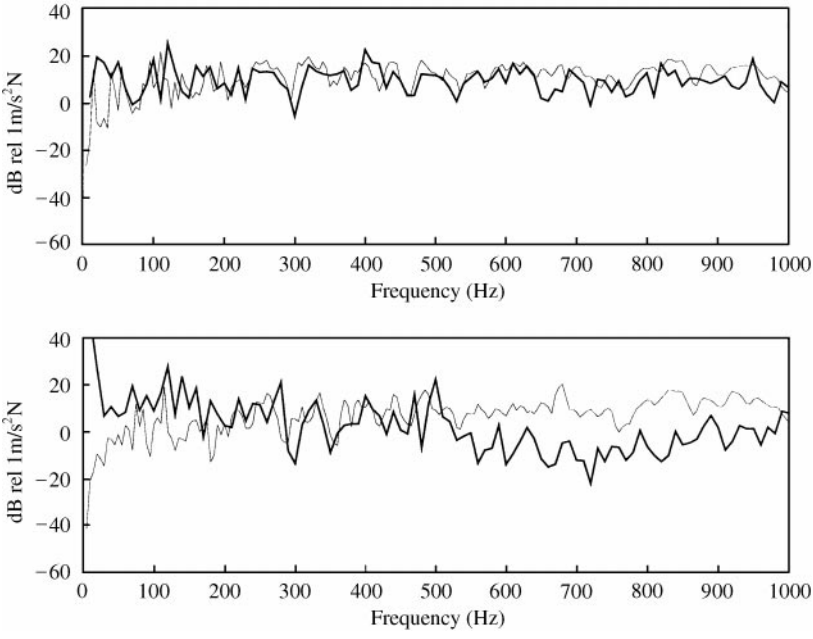

Figure A6. Estimate of the receiver K_{Er} kinetic energy without (top plot) and with (bottom plot) active control of the out-of-plane velocities at the receiver mounts junction when the primary force F_{p3} is exciting the two-panel system with three-aluminium mounts having block masses at the ends: ———, experimental predictions, ——, simulations assuming the mount element freely suspended.

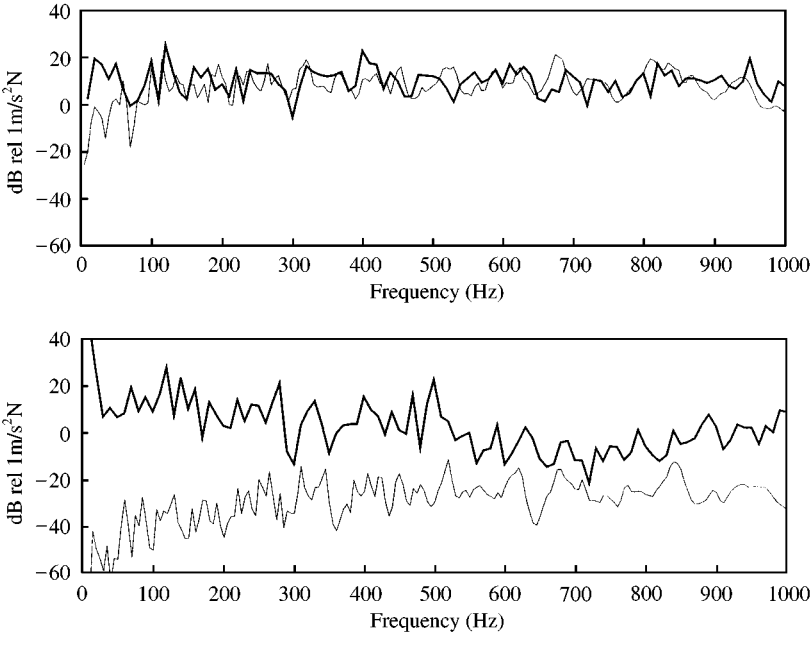

Figure A7. Estimate of the receiver K_{Er} kinetic energy without (top plot) and with (bottom plot) active control of the out-of-plane velocities at the receiver mounts junction when the primary force F_{p3} is exciting the two-panel system with three-aluminium mounts having block masses at the ends: ———, experimental predictions, ——, simulations assuming the mount element pinned in x and y directions.

ends, the four impedance matrices $\mathbf{Z}_{11}$, $\mathbf{Z}_{12}$, $\mathbf{Z}_{21}$ and $\mathbf{Z}_{22}$ assume the following form:

$$\mathbf{Z}_{11} = \begin{bmatrix} Z_{Nzw}^{S2S2} + \mathrm{j}\omega W & 0 & 0 \\ 0 & Z_{Mx\theta x}^{S2S2} + \mathrm{j}\omega I_x & 0 \\ 0 & 0 & Z_{My\theta y}^{S2S2} + \mathrm{j}\omega I_y \end{bmatrix}, \quad \mathbf{Z}_{12} = \begin{bmatrix} Z_{Nzw}^{S2S5} & 0 & 0 \\ 0 & Z_{Mx\theta x}^{S2S5} & 0 \\ 0 & 0 & Z_{My\theta y}^{S2S5} \end{bmatrix},$$

(B30, B31)

$$\mathbf{Z}_{21} = \begin{bmatrix} Z_{Nzw}^{S5S2} & 0 & 0 \\ 0 & Z_{Mx\theta x}^{S5S2} & 0 \\ 0 & 0 & Z_{My\theta y}^{S5S2} \end{bmatrix}, \quad \mathbf{Z}_{21} = \begin{bmatrix} Z_{Nzw}^{S5S5} + j\omega W & 0 & 0 \\ 0 & Z_{Mx\theta x}^{S5S5} + \mathrm{j}\omega I_x & 0 \\ 0 & 0 & Z_{My\theta y}^{S5S5} + \mathrm{j}\omega I_y \end{bmatrix}.$$

(B32, B33)

where W is the weight of the top or bottom block masses, I_x and I_y are the mass moment of inertia with reference to the x- and y-axis of the system of reference placed at the mount ends.

The excitation matrices $\mathbf{V}_m$ used in equations (55) or (56) relates the force and moment parameters at the mounts junctions to the single inertial control axial force or the pair of reactive axial forces acting on each mount. As shown in Figure A2 the reactive or inertial control excitation are modelled as acting at each end of the mounts so that the excitations sub-matrix V_1 has the following form

$$\mathbf{V}_1 = \begin{bmatrix} 1 \\ 0 \\ 0 \end{bmatrix}. \tag{B34}$$